ABSTRACT

Title of Document:	DEVELOPMENT OF AN ADVANCED ADHESION TEST FOR POLYMER INTERFACES
	Nathan Andrew Vickey Master of Science 2007
Directed By:	Professor Bongtae Han Department of Mechanical Engineering

The bond strength of polymer interfaces within packaged microelectronic devices significantly influences their reliability. In the interest of predictive modeling and to facilitate materials selection during the design process, it is highly desirable to be able to distinguish between the adhesive performances of multiple polymer interfaces. However, typical adhesion testing is normally plagued by large deviations in its test results which make drawing statistical conclusions from adhesion strength data difficult. To remedy this, an investigation into the primary sources of variance associated with the pull test was performed. Four primary factors were identified, load alignment, loading rate, bond thickness, and the edge condition. The control of each of these four parameters was targeted during the development of an improved adhesion test technique. The results are an adhesion measurement method which has successfully reduced the scatter in test results from a standard deviation of 50% to approximately 10%.

DEVELOPMENT OF AN ADVANCED ADHESION TEST FOR POLYMER
INTERFACES

by

Nathan Andrew Vickey

Thesis submitted to the Faculty of the Graduate School of the
University of Maryland, College Park, in partial fulfillment
of the requirements for the degree of
Master of Science
2007

Advisory Committee:
Professor Bongtae Han, Chair
Associate Professor Patrick McCluskey
Assistant Professor Teng Li

Table of Contents

List of Figures

v

CHAPTER 1: BACKGROUND AND MOTIVATION

1.1 Reliability of microelectronics packaging

The study of the reliability of microelectronic components continues to be of utmost importance as design requirements demand that they continually become smaller, faster, and cheaper. As microelectronics become more integrated into daily life, however, they are increasingly subjected to harsh environments that mechanically attack the electrical interconnections which make them work. Yet their growing ubiquity makes their reliable performance now more important than ever. Such stringent design constraints give rise to challenging engineering problems in the discipline of microelectronics reliability engineering which must be solved if the incredible advancements of the microelectronics industry are to continue.

Microelectronic packages are made up of plethora of internally individualized packaged components which in turn comprise of a number of both organic and inorganic materials with widely varying mechanical properties. Often failure in an electronic package, and consequently the entire device, may be attributed to a mechanical failure at a single site. Organic-inorganic bimaterial interfaces are especially susceptible to failure due to their large differences in modulii and coefficients of thermal expansion (CTEs). Several organic-inorganic interfaces are identified in Figure 1-1.
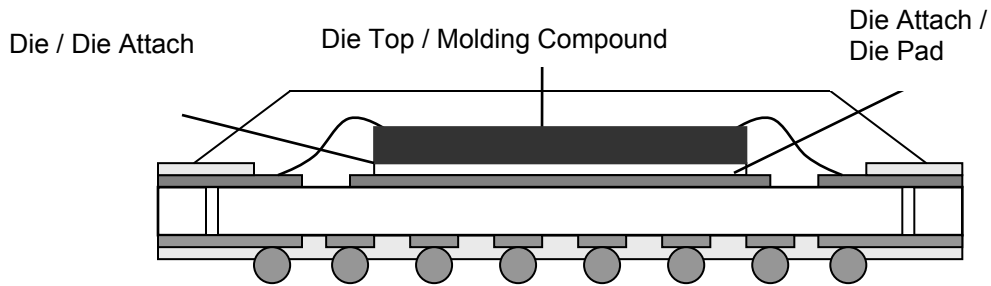
Figure 1-1: Organic/inorganic interfaces within a typical plastic ball grid array (PBGA) electronic package

1.2 Causes of polymer interface delamination in microelectronic packages

Delamination and subsequent failure along a polymer interface occurs when forces acting along the interface match and then exceed the adhesive forces that bind it. As such, the occurrence of delamination failure is a function of both the external forces on the interface and the strength of the bond itself. This means that both parameters must be well understood and characterized if one wishes to develop an appropriate predictive reliability model of a package based on a set of anticipated environmental and operating conditions. The following sections give a brief overview of the primary phenomena by which increased stresses are imparted on the bond or ways in which the adhering forces are weakened.

1.2.1 Coefficient of Thermal Expansion (CTE) mismatch

The difference in CTEs for packaging components is one of the primary causes for failure in electronic packages. This discrepancy is most pronounced along interfaces comprising of organic and inorganic materials due to their typically large CTE

mismatch. For example, the CTE for a silicon die is about 3 ppm/ °C while the CTE

for the PCB is approximately 22 ppm/ °C [1]. As depicted in Figure 1-2 for a flip

chip package, the mismatch causes each material to expand at a different rate

inducing tensile and shear stresses along the bimaterial interface which could lead to

an underfill delamination. This becomes problematic at high temperatures that the

component experiences during its normal operational. .

Silicon Die (3 ppm/ °C)

PCB (22 ppm/ °C)
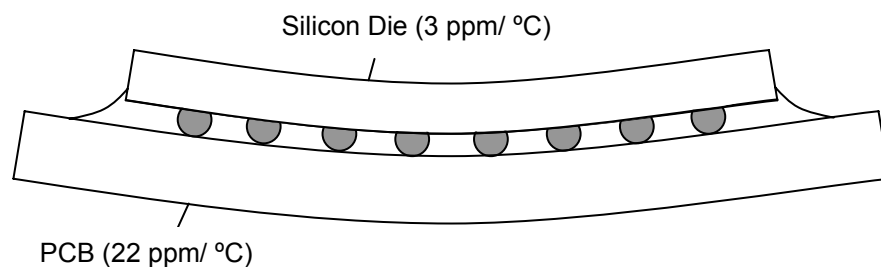
Figure 1-2: Bending of a flip chip assembly caused by CTE mismatch between
Printed Circuit Board (PCB) and Silicon Die

Additionally, the thermal mismatch problem persists in the form of low cycle fatigue

throughout the life of the package from the repeated heating and cooling cycle that

accompanies the powering up and down of the device. Over time, this thermal

fatigue induces crack growth along the relatively weak organic/inorganic interfaces

initiating delaminations and possibly causing immediate electrical failure.

1.2.2   Hygroscopic swelling

Thermal mismatch stresses may be additionally accompanied by stresses induced by

hygroscopic swelling when the package components absorb moisture from their

environment causing them to expand at different rates, analogous to the way their

volumes increase at differing rates when heated or cooled. And it has been shown that hygroscopic stresses are actually on the order or even greater than stresses generated by CTE mismatches [2]. Consequently, hygroscopic effects need to be taken into consideration as seriously as CTE mismatches.

1.2.3   Vapor pressure

When absorbed into organic materials in a package, moisture begins to fill any small cracks or voids that exist throughout. As the temperature inside the package is increased, this moisture begins to change state creating vapor pressure stresses within the device further increasing the load along the interfaces and expediting the crack growth process. This is the root cause of the common well-known occurrence of 'pop-corning' that occurs during the manufacturing process.

1.2.4   Moisture degradation

The two aforementioned causes for delamination describe how moisture ingress can induce failure by increasing the stress along an interface beyond the interfacial strength of the bond. However, in addition to increasing stresses on an interface by means of hygroscopic swelling and vapor pressure effects, moisture ingress into a package may also have a deleterious effect on the adhesion between the two interface materials, thereby reducing the maximum load that the bond can withstand. Because of moisture's ability to attack the integrity of an adhesive bond, the study of moisture on the reliability of electronic packages has recently become a topic of significant

research interest [3 - 5]. As a result, knowledge of the precise effects of moisture on adhesion has become an object of desire in the electronics packaging reliability community. To ascertain this knowledge, a suitable measurement technique must be employed to evaluate the adhesion between two materials. This measurement technique must be statistically precise enough to confidently differentiate between the mean adhesions of different bimaterial interfaces and mean adhesions of identical bimaterial interfaces exposed to contrasting environmental conditions. The remainder of this work will examine the study of the measurement of adhesion.

1.3 Terminology and mechanisms of adhesion

ASTM defines adhesion as "the state in which two surfaces are held together by interphase forces which may consist of chemical forces or interlocking action, or both. [6]" It is the force of adhesion that supplies the bonding force in an adhesive joint, defined as the location at which two adherends (a body held to another body by an adhesive) are held together with a layer of adhesive (a substance capable of holding materials together). The total adhesion of an adhesive joint is usually a combination of two kinds of adhesion; mechanical adhesion (adhesion by physical interlocking action) and specific adhesion (adhesion by intermolecular forces of a chemical or physical nature). [7]

Specific adhesion can be broken down into a number of separate adhesion theories that contribute to the overall specific adhesion of a bonded joint. They are physical adsorption theory (van der Waals forces), chemical bonding theory (covalent, ionic,

5

or hydrogen bonding), diffusion theory (polymer interdiffusion), and electrostatic theory (which is less applicable to polymers). The effectiveness of mechanical adhesion is dependent upon the surface roughness and porosity of the two adherends, whereas specific adhesion is a function of the surface chemistry between the adherends and adhesive. [7]

Specific adhesion describes the energy required to break chemical bonds at the weakest plane in the film-substrate adherent system. All other contributing factors simply modify this intrinsic adhesion. These factors include stress in the film or coating, thickness and mechanical properties of the coating or substrate, work consumed by plastic deformation or viscous dissipation, and the rate of applied testing force to the bond. All of these factors combine to produce what is called "overall practical adhesion" of the adhesive system. Overall practical adhesion is the property measured by an adhesion test and is highly dependent on all of these factors making consistent specimen preparation for adhesion testing an important and formidable task. [7]

1.4 Measuring adhesion

There are literally hundreds of documented forms of the adhesion test, ranging from extremely sophisticated configurations such as the electron spin resonance test to extraordinarily simple ones like the pull test [8]. It is important to keep in mind that all adhesion tests only measure a particular adhesive joint's performance on that particular adhesion test. Adhesion itself is not a quantifiable intrinsic property for a

given adhesive/adherend pair, but merely just a force that binds two surfaces together. Thus, any measurement of "adhesion strength" should not be thought of or applied as an innate property of the bimaterial interface of interest, but rather needs to be qualified by disclosure of the particular measurement technique used at the time as well as the individual experimental parameters that were in place. The numerical values that the test yields should be correlated with the in situ failure statistics of the adhesive joint of interest to determine how well the adhesion test relates the performance of an adhesive joint in actual use.

Although there are numerous adhesion tests, some are more routinely used than others. Four of the most common are shown in Figure 1-3: the peel test, lap shear test, blister test, and the pull test. The pull test is shown in Figure 1-3(a) and is the simplest and least inexpensive. The test comprises of two connecting rods joined in the middle by the test adhesive. When the rods are moved in opposite directions a force normal to the bondline is induced resulting in predominantly pure tensile stress along the bondline.
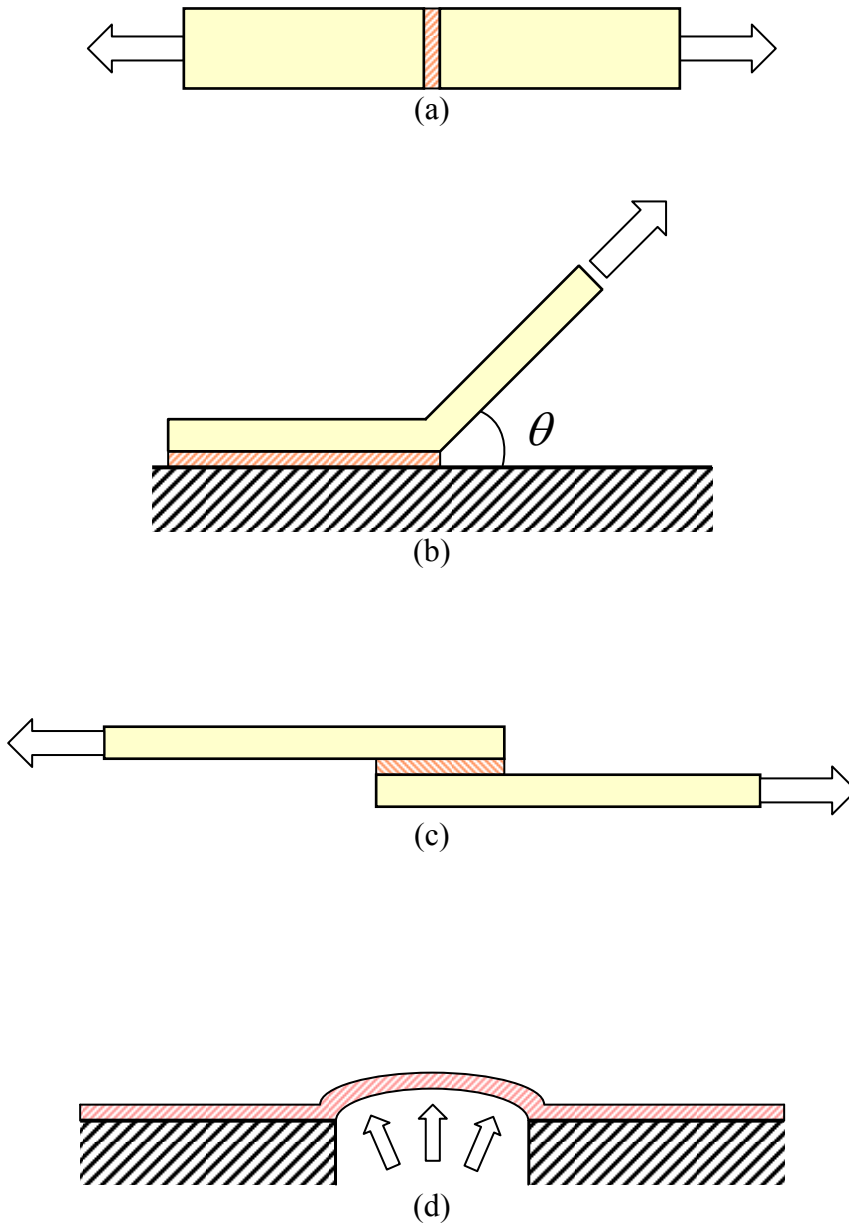
Figure 1-3: Common adhesion test methods are the (a) pull test, (b) peel test, (c) single lap shear test, (d) blister test

The force at which the joint ruptures is recorded and divided by the area of the bond to yield an average failure stress which is reported as the pull off strength [9]. The peel test is shown in Figure 1-3(b) and is somewhat more complex than the pull test in that it requires a more careful specimen preparation and complicated testing fixture. In the peel test, the flexible adherend on top is peeled away while the force applied is recorded in conjunction with its displacement to characterize the peeling strength of the adhesive. Figure 1-3(c) depicts the single lap shear test which is nearly identical to the pull test except for the slightly modified loading arrangement of the joint. As its name suggests, the lap shear test is performed by overlapping two flat adherends bonded by the test adhesive and pulling them apart until the bond breaks. The lap shear specimen is simple to prepare but obtaining precise test results is difficult due to the large number of variables that must be carefully controlled as well as the complex stress distribution that results along the bondline from the induced moment [7]. And finally the blister test is illustrated in Figure 1-3(d). Preparation of blister test specimens is undoubtedly the most difficult of the four adhesion tests introduced here. Preparation of blister test specimens requires careful etching of a small region of the underlying substrate under which the adhesive or coating sits. The pressure applied through the opening and the exact size of the subsequent bubble must be carefully monitored and then an interpretation of the complex loading and failure modes of the blister test must be evaluated. Blister testing does not work for very high strength adhesives since they are often too brittle for measurable bubbles to develop. It is therefore a more appropriate test for ductile coatings.

9

Based on the review of these common adhesion test methods, the pull test was selected as the adhesion test for modification primarily due to its inherent simplicity and intuitive measure of adhesion making it a more suitable technique for redesign. A primitive pull test can be performed with existing laboratory equipment such as a tensile tester and two metal rods bonded by the adhesive of choice. A further exploration of the pull test will be subsequently discussed.

1.5 An introduction to the pull test and challenges faced

The fundamentals of the pull test were previously addressed, however it will be discussed in further detail here since it is the primary test method of interest. Like all adhesion tests, the pull test suffers from scatter in its results due to inherent inconsistencies in specimen preparation and its testing procedure. The ASTM standard for pull testing cites acceptable differences in adhesion test results of up to 41% for intralaboratory testing and up to 58.7% for interlaboratory testing [10]. Such large scatter in test results makes it difficult to draw statistically confident conclusions between sample means. Further, large test results variance precludes the parametric study of how an additional variable in the system like moisture exposure or the fatigue of an adhesive joint affects adhesion. For these reasons, development of an adhesion testing technique with significantly increased precision is highly valuable. The following sections will outline the major problematic experimental parameters that are typically associated with the pull test and should be carefully considered during the redesign of the test.

1.5.1 Load alignment

When applying a force to the test fixture, it is desirable that the stress on the interface be nearly uniform to ensure the most consistent data possible. However, if the loading is eccentric, this will cause an uneven stress along the bondline creating a moment and shear stresses. If the eccentricity of the loading is not maintained between trials, it will result in an inconsistent measurement. As a result, numerous attempts at designing loading fixtures for the pull tests have been made to achieve proper alignment [10]. This can be difficult to achieve depending on the type of pull test being utilized, such as those that make use of tensile testers which must be retrofitted with special mechanical fixtures. Or they may prove to be very cumbersome to routinely implement requiring repeated calibration and alignment.

1.5.2 Loading Rate

Due to the viscoelastic nature of polymers, the effective modulus of the adhesive will change with the applied loading rate. If the loading rate is not consistent between trials, differing effective modulii derived from the same adhesive will characterize the joint's adhesion.

1.5.3 Bond geometry

In all adhesion testing techniques, the preparation of the adhesive bond geometry is extremely important for results consistency. Adhesive bond thicknesses have been shown to influence adhesion strength as measured by the pull test [11]. In addition to

the possible variation of the bond thickness between trials, it is also important that the bondline thickness be uniform in each trial. If this is not ensured, it becomes difficult to apply the tensile load perpendicular to the bondline in all locations, instead promoting misalignment and the formation of moments and shear stresses. Examples of bondline thickness related inconsistencies are shown in Figure 1-4(a).
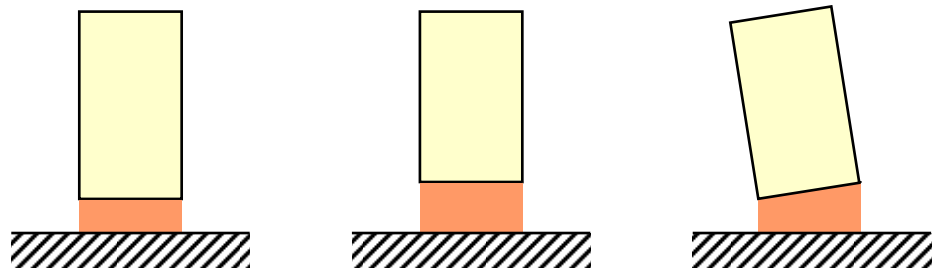
(a)
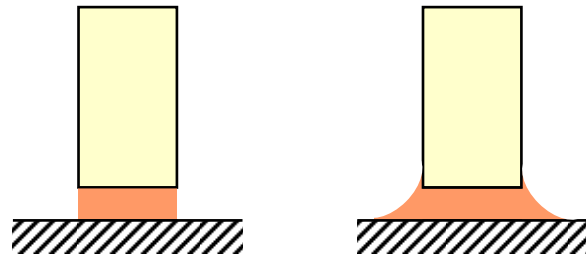
(b)

Figure 1-4: Examples of bond thickness variations are depicted in (a) while (b) shows the edge effects of bulk adhesives

In addition to bond thicknesses effects, another significant concern in relation to bond geometry is the existence of theoretical stress singularity points that exist at the bond termini [12]. These stress concentration points are highly susceptible to small microscopic changes in the bond geometry such as surface defects and contaminants on one of the adherends which are difficult to consistently reproduce and are often attributed as sources of crack formation and delamination [13]. In the case of liquid bulk type of adhesives, stress risers develop as a result of any small deviations in the adhesive geometry that might be attributed to changes in the outflow pattern of the of the adhesive as depicted in Figure 1-4(b). It is impractical or exceedingly difficult to be able to accurately reproduce this geometry and the microscopic variations that accompany it. It is preferable if the problem can be avoided altogether.

1.5.4 Other confounding variables

Numerous other variables also contribute in varying degrees to the scatter observed in pull-type adhesion testing. A short list of chemical and mechanical sources of error during the surface preparation of adherends include the existence of surface contaminants or the surface roughnesses, the humidity levels during both sample preparation and testing, the moisture conditions during sample preparation and testing, the ambient temperature during sample preparation and testing, or the consistency of the adhesive formulation used between trials and sample sets.

1.6 Motivation for work

There is a need for adhesion measurement to facilitate the predictive modeling used in the development of electronic packages which relies upon difficult to ascertain values of adhesion between polymer interfaces. Current adhesion test data is marred by excessive error, making adhesion characterization difficult. For example, it is known that the fatigue life of packages is dependent on adhesion [14]. However, due to the inherent variability associated with adhesion testing, a complete understanding between the two is difficult to establish. The benefit of improved adhesion testing is not only the ability to resolve smaller differences in adhesion strengths but also a reduction in the number of tests required, which would be especially useful when time or resources do not allow for a large number of test samples. The decrease in data required would also facilitate the ability to perform parametric analyses on a particular adhesive joint to observe the effect of other variables such as fatigue or moisture degradation on adhesion strength. Both of these would be of significant value towards the goal of improving package reliability predictive modeling. Currently such parametric studies are impractical to perform due to the number of trials that must be prepared and the precision needed to draw any form of confident conclusion from the results.

1.7 Objective of work

The objective of this work is to improve the pull-test type adhesion test technique in such a way that the scatter associated with conventional adhesion testing is significantly reduced. With reduced scatter in test results, the amount of confidence

in the mean of any sample set can be increased while the number of trials that must be performed to achieve this confidence is decreased, facilitating meaningful comparisons between sample sets. Finally, it is the goal of this work to improve the pull test in such a manner that it continues to be easily implemented and routinely practiced.

CHAPTER 2: ADVANCED ADHESION TEST

2.1 Design concepts

In an attempt to improve the consistency of the adhesion test, major contributing factors to the variability in adhesion strength were identified and addressed in the new experimental procedure. The major areas of focus were the loading alignment, bond geometry control, and loading rate control. The following sections detail how each one of these factors was controlled in the design of the new test with a focus in reducing results variability in mind.

2.1.1   Load alignment

To control the load alignment of the pull test, a pneumatically actuated self-aligning loading fixture was used. The fixture is commercially available and is described in Section 2.2.2. To operate the self-aligning tester, first a threaded bolt shaped stub is attached to the substrate of choice as shown in Figure 2-1(a). Then the bottom half of the adhesion tester is placed around the stub so that the threads of the stub protrude through the center of the tester as depicted in Figure 2-1(b). Next, as illustrated in Figure 2-1(c), the reaction plate is screwed to the top of the stub so that it is rigidly attached. Finally, air is forced into the chamber of the tester which pushes against the flexible gasket of the tester forcing apart the reaction plate and the bottom of the tester as shown in Figure 2-1(d).
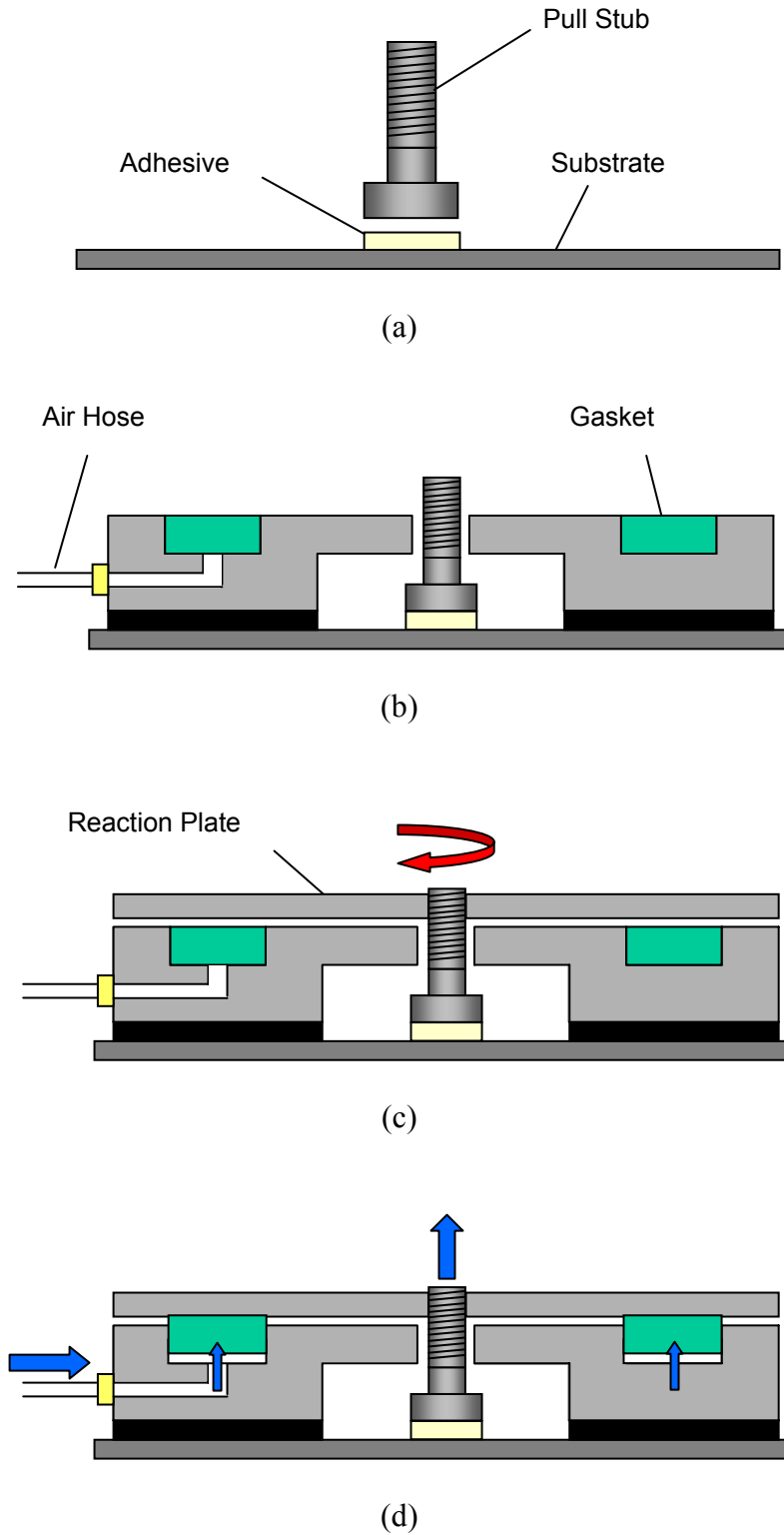
Figure 2-1: Operation of the PATTI pneumatic adhesion tester. (a) Attach stub to substrate (b) Place piston body over stub (c) Screw reaction plate to stub (d) Pressurized chamber acts perpendicular to gasket

The adhesion tester is standardized by ASTM [10] and ensures an aligned load along the axis of the stub. The alignment is a result of its pneumatic actuation since the air pressure inside the chamber will always act evenly over the entire surface of the gasket. The advantage of this is that in addition to achieving consistent alignment along the stub axis, it does this automatically, thereby eliminating the need for complex mechanical calibrations beforehand. However, it should be noted that it is necessary that the bondline be of uniform thickness or else the stub will not attach perpendicularly to the substrate. As the tester pulls the stub along its axis, the result would be an induced moment at the substrate/adhesive bondline. Therefore it is important that an even bond thickness is used. To ensure a proper bond thickness, a tilt stage is used to initially align the stub parallel to the substrate, the procedure for which is fully described in Section 2.3.3.

2.1.2 Loading rate

As mentioned above, the type of pull tester chosen for the system is powered pneumatically in a way in which the applied pneumatic pressure is proportional to the force applied to the test stub. Therefore, the challenge of controlling the force on the stub reduces to the ability to accurately control the air pressure delivered to the tester. To accomplish this, the manufacturer supplied the loading fixture with a control unit using a needle valve to adjust the orifice size and rate of gas flow from a pressurized air chamber inside to the tester. When a test is performed, a check valve is opened and an LCD display connected to a pressure sensor shows the last maximum pressure delivered to the tester. Therefore, when the specimen breaks, the LCD shows the

highest pressure that was delivered to the PATTI device which is used as the burst pressure. However, in an effort to obtain the most consistent adhesion test results possible, this arrangement poses several problems.

The first problem was that that the needle valve lacks the sensitivity to achieve a reproducible loading rate since small changes in the needle position result in significant loading rate changes. Another problem was that there is no way to actually verify the loading rate that was used in a particular test since the control unit only displays the final burst pressure. And thirdly, because the control unit is designed with portability in mind, it uses a high pressure CO_2 cartridge as a source for pressure. As a consequence, due to the finite amount of gas in the CO_2 cartridge, this pressure will vary over time as the amount of stored CO_2 diminishes which causes a change in the loading rate for a given orifice size determined by the needle valve position. Because of these factors, the vendor supplied control unit was unsuitable for the purpose of maintaining a consistent loading rate.

As a result, a new pressure control method utilizing a PID pressure controller was implemented in its place. The new controller makes use of an internal sensor to dynamically monitor the outlet pressure to the adhesion tester and makes adjustments using PID control to manipulate pulse modulated solenoid valves to regulate airflow into and out of the controller. It is operated via PC making it fully programmable and capable of recording the pressure history supplied to the tester, greatly aiding precise identification of the final burst pressure.

2.1.3 Bond geometry

As mentioned, variations to the bond geometry such as its thickness, evenness, and edge perturbations resulting from outflow of the adhesive contribute to the scatter of adhesion strength data. To resolve the problem of the edge condition, a novel technique has been developed. The new technique controls the interface geometry in a way that dominates failure and negates the influence of the edge condition. To achieve this, an artificial crack of known size is induced along the bondline before testing as shown in Figure 2-2. Ensuring that this crack is larger than the inherent flaw sizes in the adhesive and along the bond's interface causes fracture to occur at the artificial crack location each time [15]. By doing this, the bond area and resulting average interface stress is controlled in addition to the mode of failure, which according to finite element analysis described in Section 3.2.2, should occur along the adhesive-substrate interface.
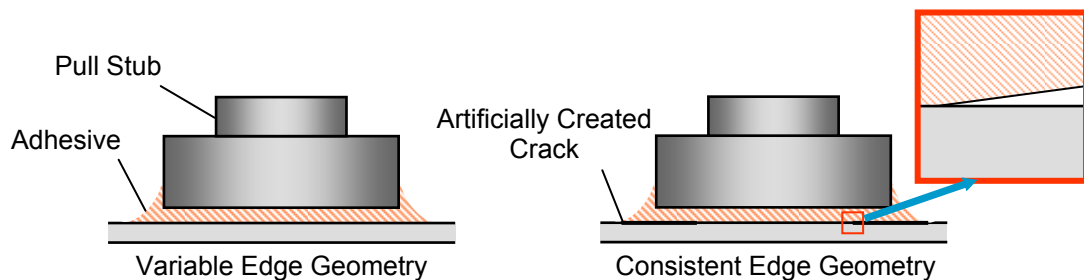
Figure 2-2: Illustration of artificial crack creation concept

The formation of the described interface crack is accomplished by spraying a layer of release agent circumscribing the center of the adhesive bond area. This is done by masking off the targeted adhesive bond area as shown in Figure 2-3(a). Then, as depicted in Figure 2-3(b), a spray gun is used to deliver a layer of the release agent

everywhere around the mask to the substrate. This serves to create a layer of low adhesion between the substrate and the rest of the adhesive. The mask is removed after spraying and the release layer is dried as illustrated in Figure 2-3(c). Once dry, the adhesive and pull stub are attached and the specimen is ready for testing. When a force is applied to the stub, the outer ring of release agent detaches from the substrate prior to the stronger adhesive bond area as shown in Figure 2-3(d). This leaves a precisely defined bond area bounded by a crack of known size and geometry. A more detailed procedure for spraying the release agent is described in Section 2.3.2.

(a)

(b)

(c)

(d)
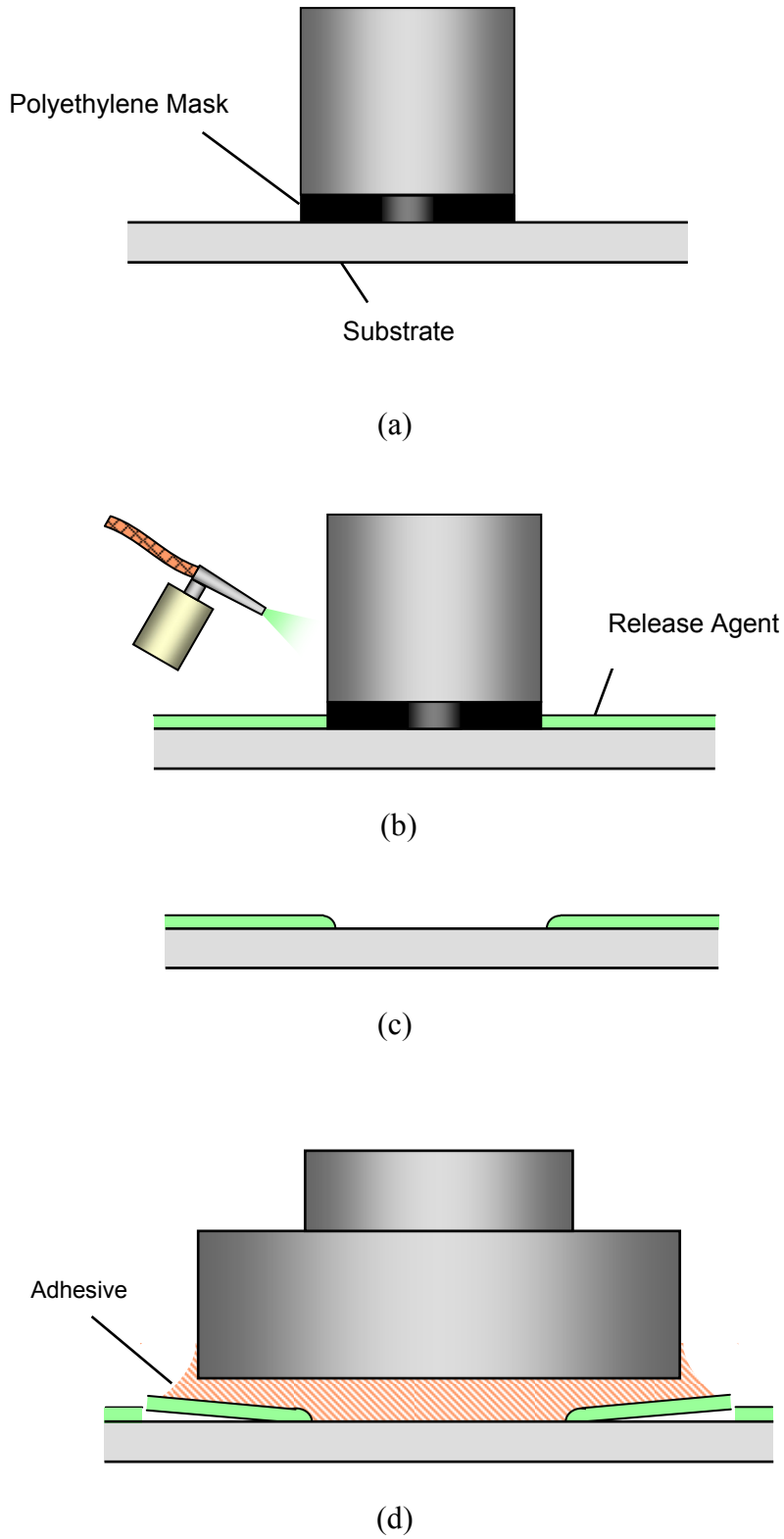
Figure 2-3: Procedure for creating interface of weak adhesion around the bond area to induce a crack of known geometry along the substrate/adhesive interface

Thickness shims were originally used to offset the stub the appropriate distance from the test substrate, but were found to be ineffective with deviations of bond thicknesses of over 100 microns. To ensure the appropriate bond thicknesses a specimen preparation apparatus was constructed utilizing a tilt stage and translation stage as illustrated schematically in Figure 2-4.

Precision Translation Stage

Positive Lock
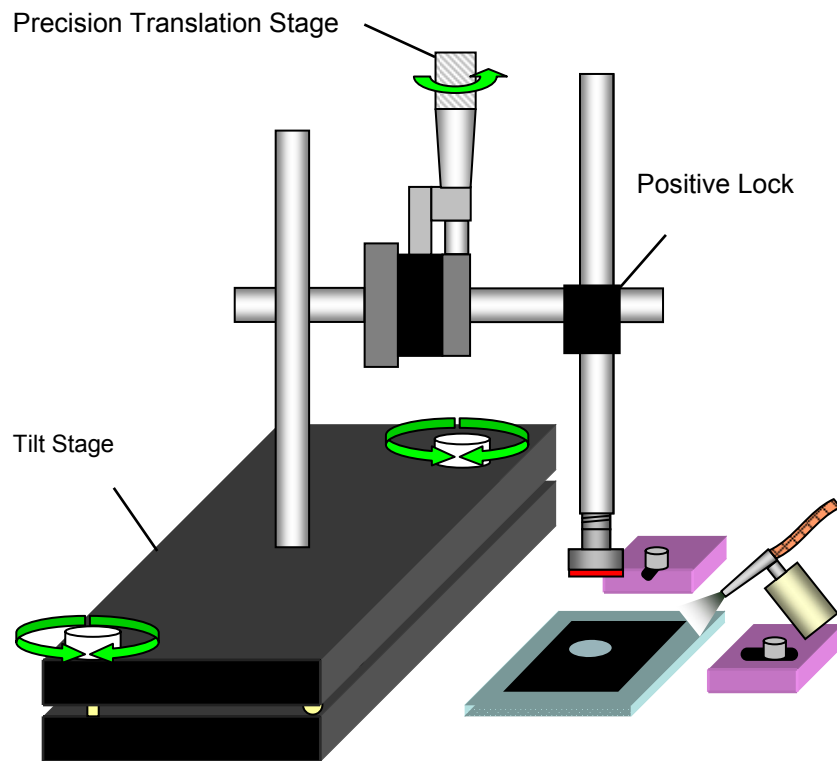
Tilt Stage

Figure 2-4: Tilt and translation stage configuration used to center mask and accurately specify bond thickness and evenness

The tilt stage ensures that the stub's face maintains parallel to the substrate while the translation stage can be used to adjust the bond thickness. Also, the specimen preparation stage is used during the application of the release agent layer as shown in Figure 2-4. The stage is fitted with alignment blocks to ensure that the masked area

of the substrate matches up concentrically with the pull stub when the adhesive is applied. A thorough description of the specimen preparation stage and its operation can be found in Section 2.2.4.

2.2 Detail of experimental equipment

A complete schematic of the full experimental setup is shown in Figure 2-5 while a photograph of the setup is shown in Figure 2-6. The major components will be described in detail in the following sections.
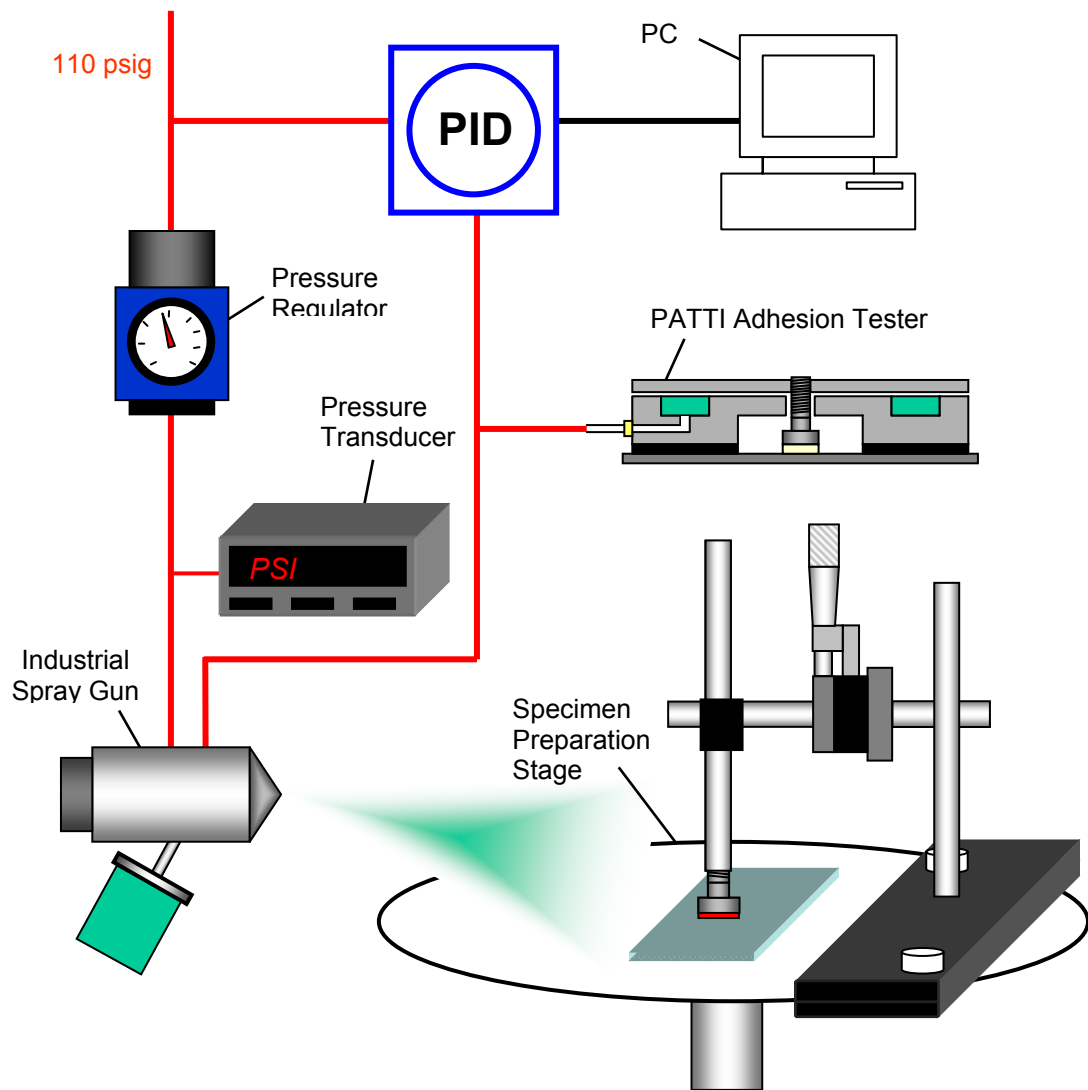
Figure 2-5: Schematic of complete experimental setup
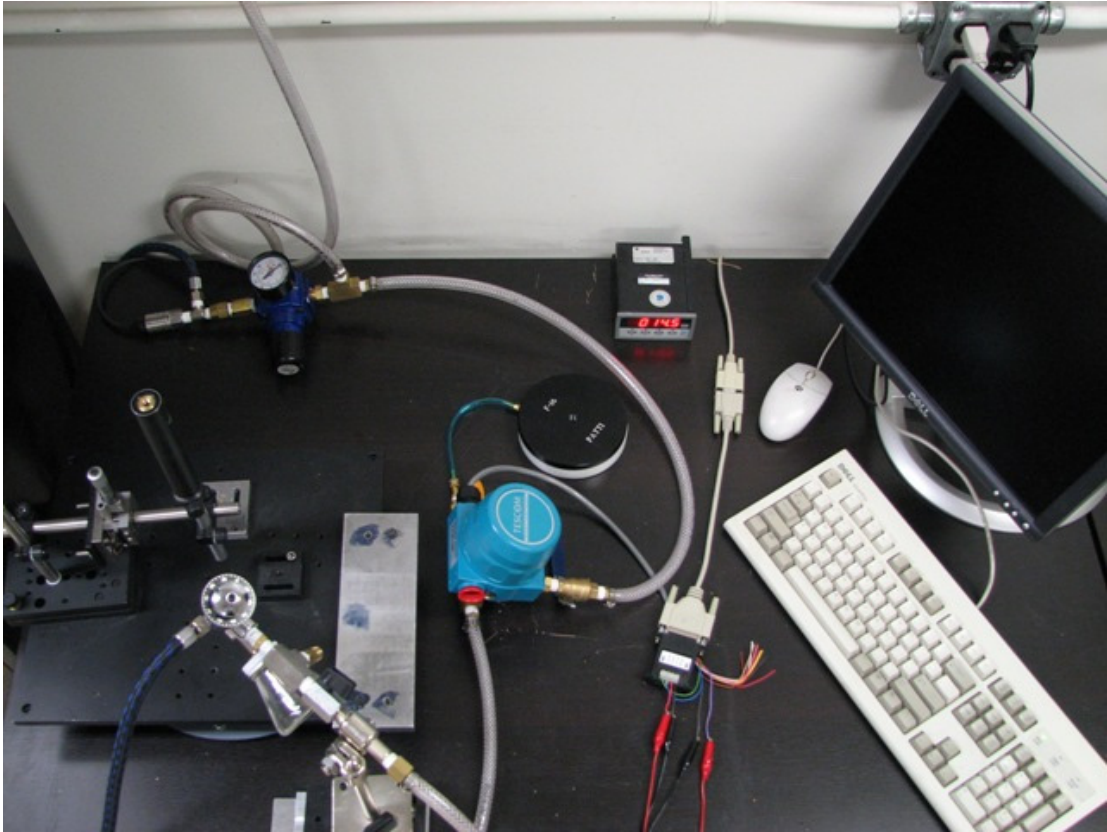
Figure 2-6: Photograph of experimental setup depicted in Figure 2-5.

2.2.1 PID controller

The PID electronic pressure controller (TESCOM Corporation; Model ER3000-SV1) has an internal pressure transducer that can be used as feedback to control the outlet pressure, which was taken advantage of in the setup. The internal sensor response time is 25 ms and the accuracy at room temperature is 0.1% of the span max. A maximum pressure of 100 psi was specified in this case yielding an accuracy of 0.1 PSI. The controller has an output range of 0 to 100 psi and is powered by a 24V DC power source. It can be connected to a computer through the serial port via a RS232 to RS485 adapter which was utilized in this setup. The controller is packaged with proprietary Windows Tune software for the PC which enables complete control of the

controller's variables, including the ability to program a loading profile into the controller. The software also enables the user to record the pressure history which is monitored by the internal pressure sensor, greatly aiding precise identification of the final burst pressure during post processing. A picture of the PID controller is shown in Figure 2-7 while the user interface of the Windows Tune software is depicted in Figure 2-8.

Figure 2-7: TESCOM ER3000-SV1 Electronic Pressure Controller used in the experimental setup
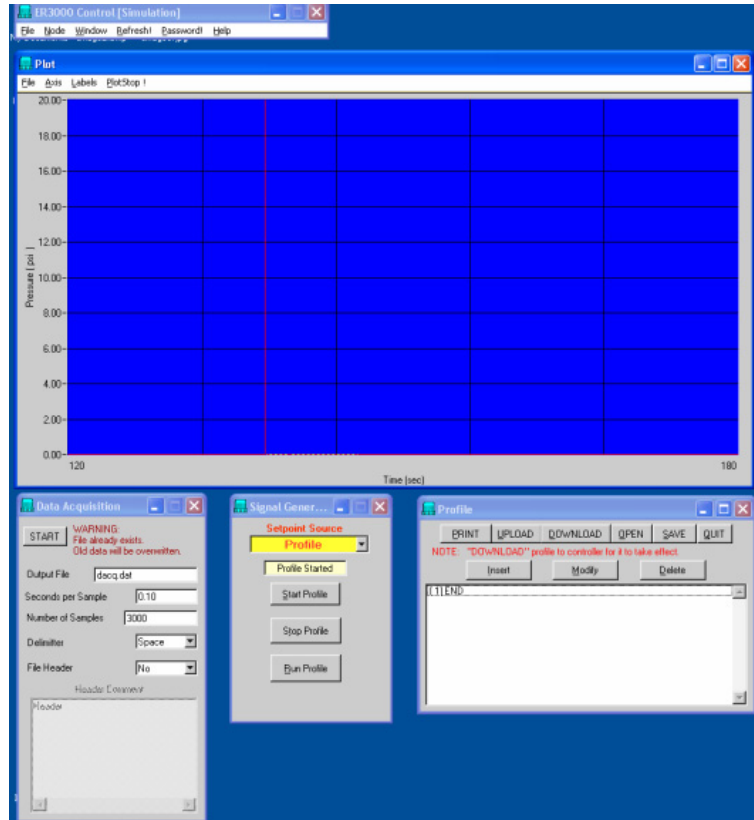
Figure 2-8: User interface for TESCOM's Windows Tune software

2.2.2 PATTI test fixture

The adhesion test fixture is part of the Pneumatic Adhesion Tensile Testing Instrument (P.A.T.T.I) System (SEMicro Division, M.E. TAYLOR ENGINEERING, INC, D 4541 – 02 [10]) for measuring the tensile strength of an adhesive by the bar and rod method, and is patented in the United States [16]. As mentioned in Section 1.5.2, only the loading fixture of the P.A.T.T.I. system was used in the development of this technique, the workings of which were described in Section 2.1.1 and shown in Figure 2-1. The loading pistons are sold in several different sizes depending on the maximum pressure needed.   In the tests conducted in the development of this technique, the F-16 piston was primarily used and is shown in Figure 2-9 in

comparison to a smaller F-2 piston which would typically be used for applications requiring a lower maximum force.
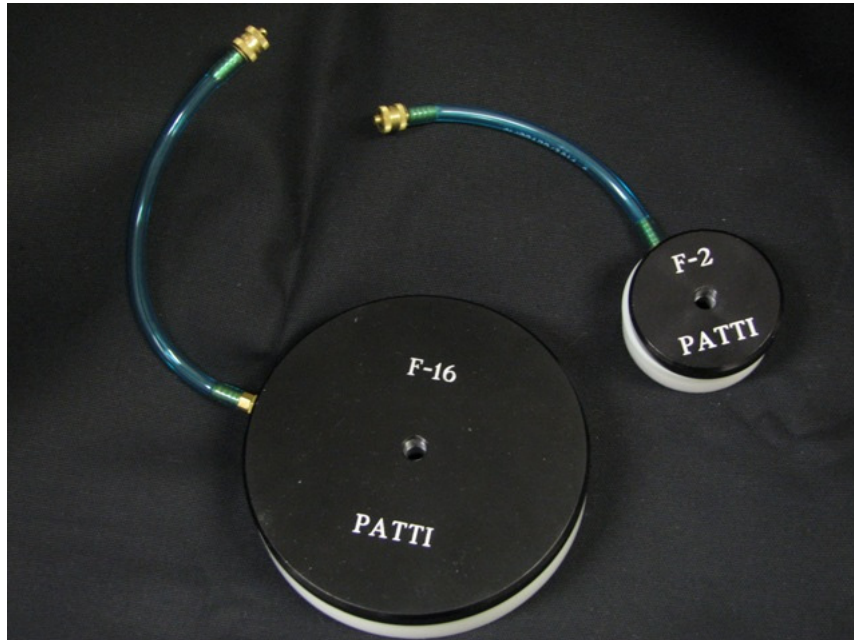
Figure 2-9: The F-16 and F-2 loading fixtures manufactured by SEMicro Division

The piston names (F-16, F-8, etc.) are derived from the surface areas of their interior gaskets. The larger the gasket area is, the greater the pressure that is transferred to the reaction plate for a given inlet pressure. The gasket area is used to calculate the average stress along the bondline between the pull stub and substrate during a test. The average stress along the bondline at the time of failure during an adhesion test is called the pull-off strength of the adhesive-substrate pair, but will be referred to as the adhesion strength for the remainder of this work for simplicity. The adhesion strength is calculated using Equation 2-1.

$$\sigma = \frac{(PA_g - W_{rp})}{A_s} \tag{2-1}$$

where the final inlet pressure into the chamber is P, the area over which the gasket acts on the reaction plate is A_g, the weight of the reaction plate is W_{rp}, and the surface area of the pull stub A_s. The pull stubs used in testing were provided by SEMicro, made of aluminum, and have a head diameter of 0.5". A picture of a pull stub is shown in Figure 2-10.

Figure 2-10: Aluminum 0.5" pull stub

2.2.3 Industrial sprayer

The spray gun (Paasche Airbrush Company; A-AUAR) with tip (AU-3) and round air cap nozzle (AR-15–3) used for spraying was rigidly mounted on a base (16-1-7). The A-AUAR spray assembly with the aforementioned tips installed is shown in Figure 2-11. The A-AUAR comes equipped with the AU-7B fluid body which has two ¼" NPT male inlet ports, one for the atomizing air stream and the other for the spray fluid. The spray gun is siphon driven, meaning that the atomizing air stream creates a

low pressure in the fluid body head siphoning out the fluid from the glass reservoir. There it is mixed in the fluid body and then atomized and propelled out through the spray tip. As a result, the spray volume is dependent on the atomizing air stream pressure. To ensure reproducibility of the spray pressure during each spray application, a pressure transducer (Druck PDCR 4010) connected to a digital indicator (Druck DPI 280) was attached to the airline between the regulator and fluid body head so that the regulator could be adjusted to the correct pressure (see Figure 2-5).

The pathway from the fluid reservoir is normally blocked in the automatic spray gun by a needle in the spray tip. The needle tip is only retracted when sufficient pressure is applied to the activation inlet of the shell assembly to push a spring supported piston back which is attached to the needle. Once the needle tip is retracted, the low pressure in the fluid body begins to siphon out the fluid from the reservoir where it is then atomized by the same air stream. In the experimental setup, the PID pressure controller is utilized to maintain easy control over the pressure in the shell assembly, thereby making it easy to control the spray time during the application of the release agent. The cylindrical cap assembly of the spray gun also possesses a dial to adjust the amount of compression in the spring inside the shell assembly. The adjustment changes the amount of distance which a given pressure will retract the needle tip which controls the orifice area. As a result, the flow rate can also be modified using the dial on the cylindrical cap. In the interest of maintaining a consistent and

repeatable release agent layer thickness when spraying, care should be taken to maintain the same atomizing air pressure, dial setting, and spray time.
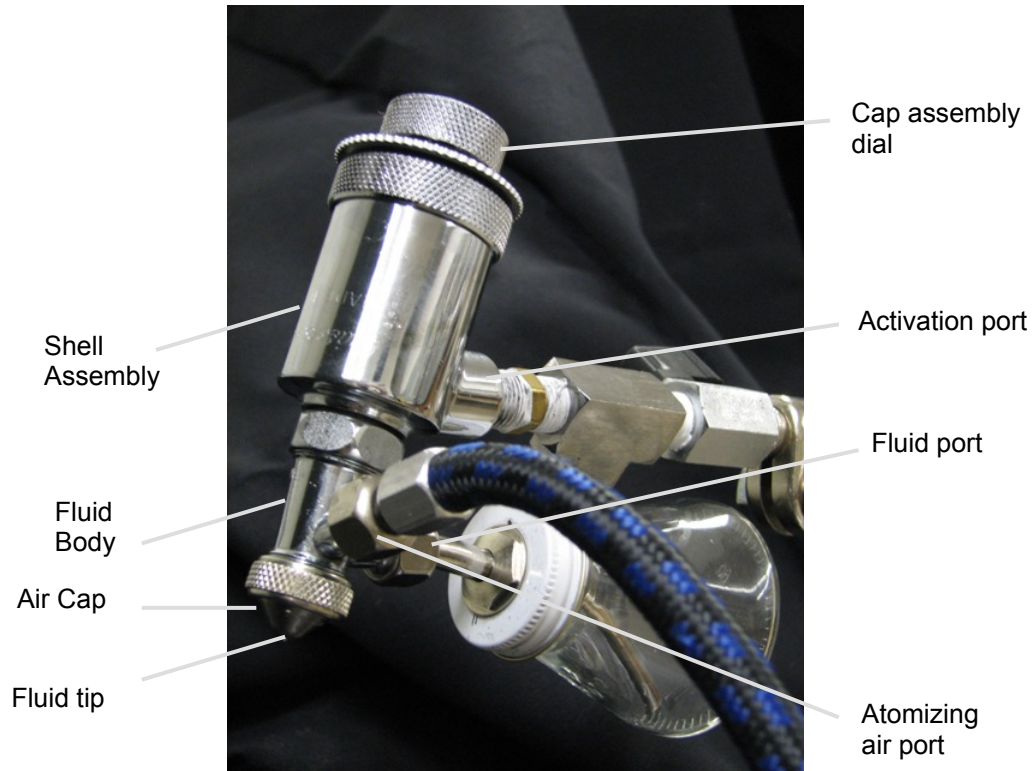
Figure 2-11: Industrial Automatic Spray Gun model A-AUAR manufactured by Paasche Airbrush Company

2.2.4 Specimen preparation stage

The specimen preparation stage is used to align the masked bond area in the center of the pull stub. During the application of the adhesive, it is also used to control the bond thickness and evenness by means of a translation stage (Newport 461 Series) driven by a one micron resolution micrometer and a two axis optical tilt stage (Creative Stars). The translation stage is able to recreate a bond thickness of +/- 10 μm. A photo of the translation stage is illustrated in Figure 2-12. The entire

preparation stage is also mounted on a rotating turntable (Paasche Airbrush TL – 12).

This is done so that the spray gun can be mounted in a fixed position while the entire

preparation stage is rotated allowing the release agent to be applied evenly from

several angles. To accomplish this, it was necessary to ensure that the axis of the stub

holder was aligned with the axis of rotation of the turntable.
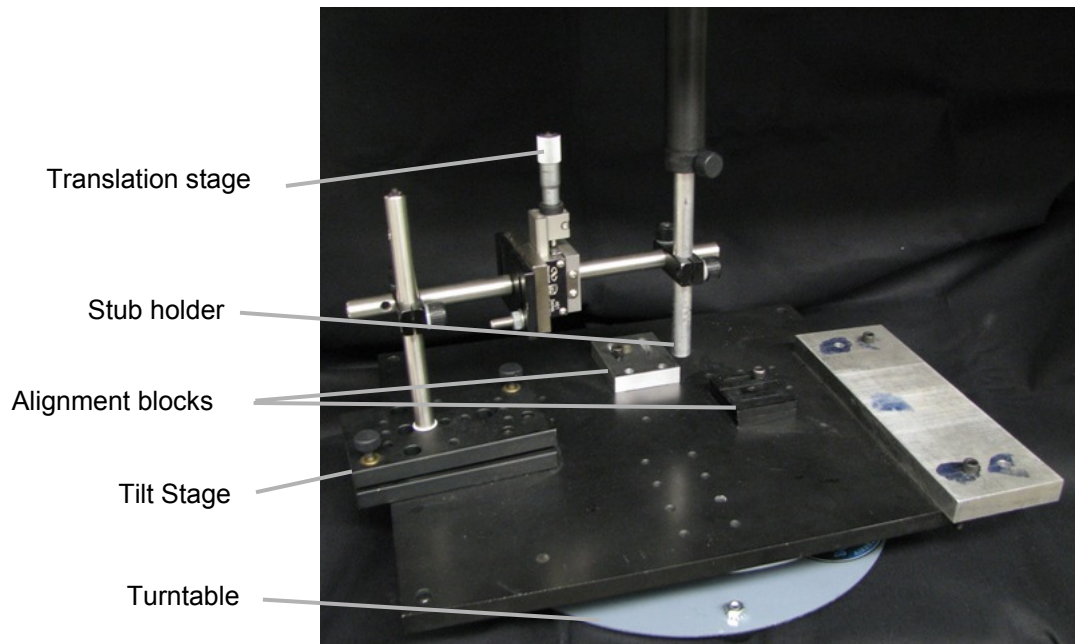
Figure 2-12: Specimen preparation stage

Two alignment blocks were mounted to the preparation stage base and were used to

align a substrate underneath the stub holder so that the substrate remained in the same

location during release agent spraying and adhesive application. This ensured that the

stub face was attached concentrically around the bond area.

When spraying the release agent, a special mask stub was screwed into the stub

holder as shown in Figure 2-13. The mask stub was created by lathing off the head of

a stub down to a diameter of 3/8" and facing off the end. Then a 3/8" diameter plastic polyethylene washer was glued to the end with the burred side facing out. Careful attention was paid when fabricating the mask stub since it is important that the washer be accurately centered along the stub axis to be sure that the adhesive bond area was centered on the ½" diameter stub. In order to accomplish this, a 3/8" hole was drilled in a small 1" x 1" x ½" aluminum block. When lathing the head of the mask stub, the diameter was incrementally reduced and checked using the aluminum block to minimize the tolerance between the two. When finished, the washer was fitted onto the mask stub using the aluminum block as a guide to ensure that it was properly centered.

Figure 2-13: Mask stub used during release agent spraying

2.3 Experimental procedure

Since the reproducibility of adhesion test data depends heavily upon the accuracy of the specimen preparation process [7], a detailed record of the procedure was made. The preparation of the adhesive-substrate system will vary slightly depending on the materials used, such as liquid type adhesives versus laminated tape type, but the primary methods are common to each. The following experimental procedure describes the steps performed to produce the data discussed in Chapter 4. The procedure will refer to several components in the experimental setup by name and Figure 2-4, Figure 2-5, Figure 2-11, and Figure 2-12 should be referenced when needed.

2.3.1 Substrate and specimen preparation

The substrates used in the experiments were 3" x 2 5/8" x ¼" Ultra Low Expansion (ULE) glass plates. Glass plates were used during the development of this experimental technique for the following reasons. First, because they are clear and allow for the observation of the polymer interface during testing which is discussed in further detail in Section 3.1.3. Second, the plates are manufactured to a high thickness tolerance with thickness deviations measuring a maximum of approximately two microns over the area of the plate. Additionally, the confounding contributions from surface roughness variations to the adhesion strength of the interface are minimized. The substrates are cleaned beforehand with acetone and lint free tissue.

The faces of the pull stubs obtained from the vendor were found to be of inadequate flatness with a difference in height from edge to center of up to 80 microns. Since the thicknesses of adhesives to be tested were on this order, all of the faces of the stubs were lathed off until no discernable height difference was detectable. All of the test stubs were also cleaned with acetone and lint free wipes before use.

2.3.2 Release agent application

The release agent mixture used in this technique consisted of a four parts polyvinyl alcohol (PVA) solution (EP7930 from Eager Plastics) and one part carbon black lamp dye by weight. The methodology used to determine this ratio is described in Section 2.4.1. After the mixture is properly weighed out and thoroughly mixed in the spray gun's reservoir jar, it is attached to the sprayer.

Next the mask stub was cleaned with acetone and then attached to the stub holder. Then the translation stage was adjusted to a position of 0.7 cm. This is done for two reasons. First is so that there is ample range left in the micrometer of the translation stage to traverse the thickness of the substrate to the base of the preparation stage for stub leveling prior to the adhesive application. The second reasons is because the translation stage must always be adjusted to a consistent position in order for the positive lock to grip the stub holder at the same position every time. If not, deviations in the straightness of the stub holder will cause the adhesive bond area's location to differ for changing grip locations. In this respect, it is also important that the rotational position of the stub holder in the positive lock be consistent. After this, the

substrate is placed flush against the alignment blocks, the positive lock is opened, the stub holder and mask stub are lowered onto the substrate and the positive lock retightened. Next the release agent is sprayed.

The settings used for spraying the release agent in all of the experiments conducted yielded a release agent layer thickness of 11 microns with a standard deviation of approximately 10%. The other parameters were an atomizing air pressure of 11 psig, cap assembly dial setting of 8.7 turns from fully open, and a dwell time of five seconds at 40 PSI stepped from 0 PSI for the activation port. The position of the spray head tip was 3" away radially from the stub holder and 5" from the surface of the preparation stage directed at the center of the stage, resulting in the spray path making a 59º angle with the surface of the preparation stage. Since small differences in these settings may cause a change in the spray thickness, it is recommended that after all of the settings are set, a few substrates be sprayed first and their layer thicknesses measured. Then the spray time may easily be modified to tune the spray system to the desired thickness since the relationship between spray thickness and spray time is linear. After all of the spray settings were set, the substrates were sprayed for five seconds at four angles separated by 90º increments by rotating the turntable. Then the stub holder was then raised via micrometer and the substrate removed. For faster drying, the substrates were placed in an oven at 75ºC for approximately 5 minutes. A picture of a substrate after the release agent layer has been sprayed is shown in Figure 2-14.
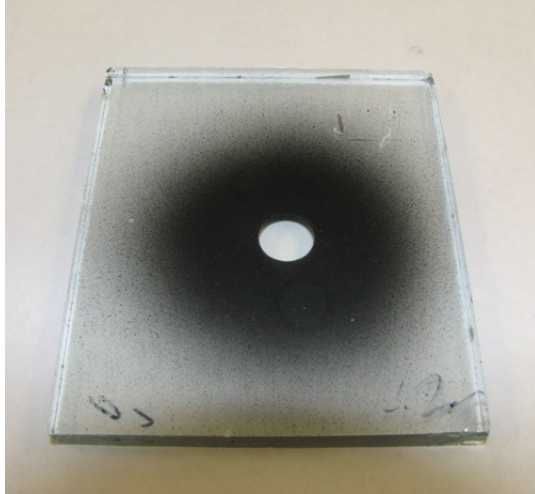
Figure 2-14: Substrate after the release agent has been applied

2.3.3   Application of bulk adhesive using the preparation stage

The experimental technique was developed primarily by testing a two part epoxy called PC-10C from Photoelastic Division, Measurement Groups Inc. on ULE glass substrates. The hardener to resin ratio by weight specified for the PC-10C adhesive was 15% which was measured using a digital scale and mixed in a test tube. The resin and hardener were thoroughly blended using a metal spatula and then centrifuged for two minutes to remove any air bubbles.

Before the adhesive is applied to the masked substrate, it must be leveled and zeroed with respect to the substrate. This was done by placing an unused substrate onto the specimen preparation stage beneath the stub holder, adjusting the micrometer position to 0.7 cm, and then lowering it to the substrate and securing the positive lock. This ensures that the stub holder is being held in the same position as it was during release agent layer spraying. After this, the stub was lowered to the specimen preparation

stage and the adjustment knobs on the tilt stage were used to level the stub with the stage. This was accomplished by using a lamp to shine a light behind the stub and then by adjusting the tilt knobs until no light could be seen between the perimeter of the stub and the preparation stage.

After the tilt was adjusted, the position of the stub relative to the substrate was zeroed by raising the translation stage back to 0.7 cm, replacing the blank substrate with the masked substrate, and then releasing the positive lock and lowering the stub to a region of the masked substrate away from the bond area. This is done so as to not to damage the release agent layer in the region where the adhesive was to be applied. After the stub made contact with the substrate, the positive lock was retightened and the translation stage raised. The bulk adhesive was applied to the area on the substrate that was originally masked, and then fitted back against the alignment blocks. The translation stage was then lowered to a position of 0.72 cm, resulting in a bond thickness of 200 microns.

It should be noted that the stub was leveled on the specimen preparation stage only because it was difficult to see where light passed through the space between the stub and glass substrate due of its transparency. If an opaque substrate were used, the leveling of the stub would have been done with respect to the substrate.

2.3.4 Application of laminated adhesives using the preparation stage

Laminated type adhesives were also characterized during the development of the technique; the results for which an Adwill LE4764 die bonding tape manufactured by Lintec are reported in Section 4.1.3. The substrates were prepared in the same manner as described in Section 2.3.2 and then placed on a hotplate heated to 110ºC. A strip of the adhesive was cut and then the cover film was removed along half of its length. The end of the adhesive from which the cover film was peeled was attached to the substrate. After which, the rest of the adhesive was attached by using a thin metal rod and sliding it across the length of the adhesive to adhere it to the substrate as shown in Figure 2-15. By doing this, the formation of air bubbles under the adhesive was largely avoided.
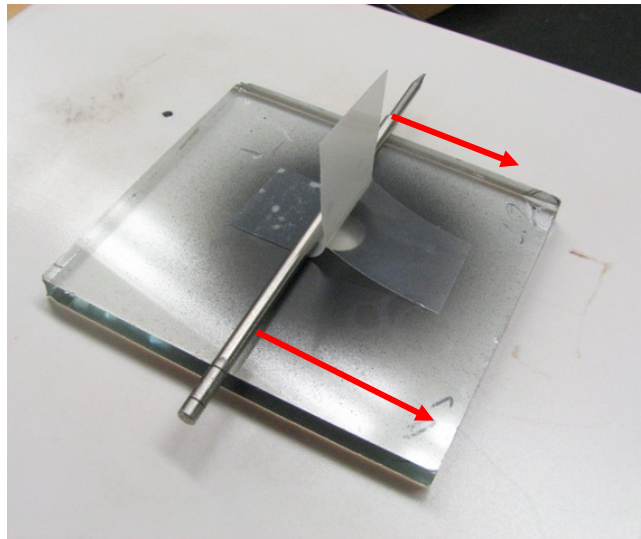
Figure 2-15: Procedure for attaching a laminated adhesive to avoid the formation of air bubbles

After the adhesive was attached, it was exposed to an ultraviolet light with a radiant flux of 860 µW for one minute. This was done to facilitate the removal of the base

film which was removed with tweezers. Next, the LE4764 adhesive was placed in an

oven at 125ºC for 30 minutes to cure. After the adhesive was allowed to cool, a test

stub was attached on top of the laminated adhesive with a quick curing epoxy using

the procedure described in Section 2.3.3.

2.3.5   Testing using PID control

For testing, the specimens were loading into the P.A.T.T.I adhesion tester as

described in Section 2.1.1. In the Windows Tune program (shown Figure 2-8), a

profile with a ramp to 18.6 PSI in 60 seconds was used, which, when converted to an

average stress over a 3/8" diameter bond area, corresponds to a ramp rate of 45 PSI/s.

The loading rate used falls into the middle of the range as specified by ASTM for pull

off type tests [10]. Finally, the profile was activated and the history from the internal

pressure sensor was logged for post-processing.

2.3.6   Post processing and analysis of results

After the samples were tested, the highest pressure obtained before delamination was

used as the burst pressure in calculation of the adhesion strength with Equation 2-1.

An example of a loading profile used in testing and how the burst pressured is

identified is shown in Figure 2-16.

Outlet Pressure (PSI) vs Time (s)
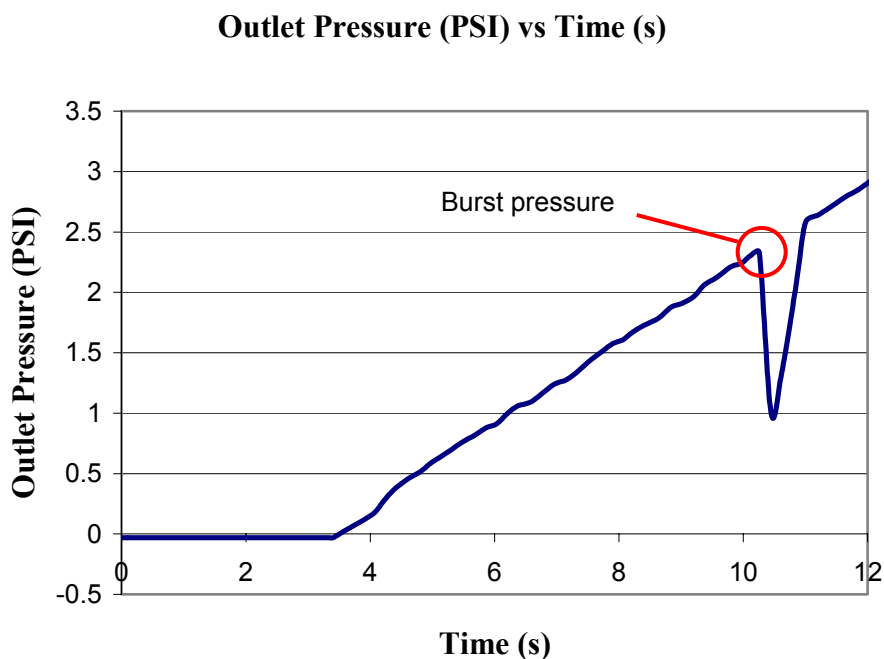
Figure 2-16: An example of the pressure history logged by the Windows Tune software and identification of the burst pressure

2.4 Technical challenges encountered

2.4.1 Over adhesion of release agent layer

As mentioned in Section 2.3.2, the final release agent mixture used in this technique consisted of a 4:1 ratio by weight of PVA to carbon black lamp dye. However, initially only PVA was used as a release agent, and as will be discussed in Section 3.1.4.1, white light interferometry was used to observe that initial delamination of the outer release agent layer was also causing a crack to propagate nearly instantaneously through the center adhesive bond area at the same time. This was undesired since in such a case the adhesion test is doing more to measure the initial force needed to initiate failure in the release agent layer than at the adhesive interface of interest.

The objective of the controlled area technique was to use a release agent layer to create a defined bond area to test the adhesive of interest. It had been assumed that the PVA layer had nearly zero adhesion or that the delamination of the release agent layer would be arrested at the adhesive boundary prior to reaching the force needed to delaminate the adhesive. But based on these observations, it was apparent that the release agent layer had a greater adhesion than originally expected. To better understand the adhesion of the release agent layer, a 15 µm layer of PVA was applied to five substrates and stubs were attached using a quick setting room temperature epoxy (Loctite QM-50) with a thickness of 200 µm. These samples were then tested using the procedure described in Section 2.3.5.

The resulting average adhesion of the release agent layer was measured to be 162 PSI. The value was larger than expected and a method to reduce the adhesion of the release agent was sought. To reduce the adhesion of the PVA, several ratios by weight of carbon black lamp dye were added to the PVA and their adhesion strengths measured in samples of five trials each. The results are shown in Table 2-1.

PVA to Dye Weight Ratio	Average Adhesion Strength (PSI)
1:1	112
2:1	64.0
4:1	< 34.6
1:0	162

Table 2-1: Average adhesion over five trials for four PVA:carbon black lamp dye ratios by weight

It was observed that the minimum adhesion strength occurred for the case of a 4:1 weight ratio. In that case, two of the five samples had adhesions that were so low that they broke during installation into the P.A.T.T.I. instrument. The explanation given for the existence of an optimum PVA to dye ratio is that for high concentrations of dye, the mixture is not able to form an adequate barrier between the substrate and adhesive, while for lower concentrations the dye has less effect. Based on these results, a ratio of 4:1 was chosen to be used for subsequent testing. Using the technique of white light interferometry described in Section 3.1.4.1, it was confirmed that by using this ratio the release agent layer would be delaminated prior to the rest of the adhesive bond area. Additionally, the opaqueness of the carbon black dye makes it easier to observe the centering of the adhesive bond area on the test stub as seen in Figure 3-6.

2.4.2 Poor contact during preparation of laminated type adhesives

The application of the developed technique to laminated type adhesives requires only a few small modifications to the aforementioned procedure which was described in Section 2.3.4. A problem encountered during the preparation of laminated adhesives

was that when attaching the stub directly to the laminated adhesive, poor contact between the two resulted. This was attributed to the 40 μm thinness of the LE4764 adhesive used and the surface topography created when attaching a laminated adhesive over the masked release agent layer. When this is done, a crater shape is formed because of the 'hole' in the release agent layer that the adhesive must fill. Since the thickness of the adhesive used was on the order of thickness of the release agent layer, this posed a problem. When a stub would be attached, it would only form good contact near the circumference and not in the center, cratered region.

To solve this problem, a secondary liquid dispensed adhesive (Loctite QM-50) was used to attach the stub to the laminated adhesive layer. By doing this, the liquid type adhesive filled the cratered region between the stub and the laminated adhesive layer ensuring good contact between the two. And this is the procedure used to prepare laminated type adhesives described in Section 2.3.4.

CHAPTER 3:   VERIFICATION AND OPTIMIZATION OF TECHNIQUE

3.1 *Use of white light interferometry in proposed technique*

3.1.1   Introduction to interferometry and white light interferometry

Interferometry is a technique that utilizes the interference between two or more electromagnetic waves to measure some physical quantity.   The fundamental principle under which interferometry operates is superposition, made possible due to the wavelike nature of light.   In a common implementation of interferometry, a laser is used to generate a coherent beam of light which is split into two beams, an active and a reference beam.   The active beam interacts with the physical system of interest which will affect its phase, while the reference beam's phase remains unchanged. When the two are recombined, their wave-fronts constructively or destructively interfere resulting in an interference pattern from which conclusions about the physical system can be drawn.   Interferometry is a valuable technique and has many implementations.   One   such   implementation   is   out-of-plane   displacement measurement which is of interest for the current application.

Common techniques for of out of plane displacement interferometry include Twyman-Green, Fizeau, and white light interferometry.   In each of these methods, the active beam's wave-front is distorted by the topography of a targeted specimen's surface.   When recombined with the reference beam, the resulting interference pattern forms a two dimensional contour map reflecting the surface topography of the specimen.   An example of such a contour pattern generated from the warpage in a

Flip-Chip package using Far Infrared Twyman-Green Interferometry (FITGI) is seen in Figure 3-1 [17].
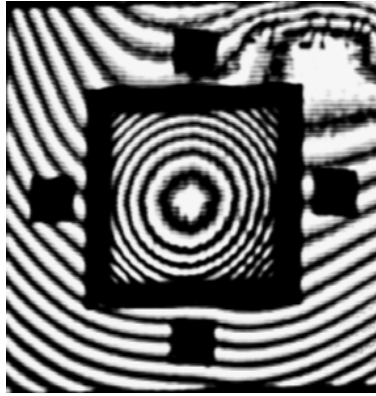
Figure 3-1: Fringe pattern of a Flip-Chip package generated by a Far Infrared
Twyman-Green Interferometer (FITGI) [17]

In the verification of this adhesion test technique, white light interferometry was the utilized procedure, the motivation for which is explained in Section 3.1.2. White light interferometry differs from Twyman-Green and Fizeau in that it does not use a monochromatic light source. Because white light is a broad spectrum source, its temporal coherence is only maintained when the optical path length (OPL) difference between interfering beams is relatively small [18]. As a result, the maximum fringe order with sufficient contrast is limited by the OPL difference. The advantage of white light interferometry is that it is easily implemented (in this case using ambient light) since there is no need for a coherent light source such as a laser and the accompanying complex optical configurations. Figure 3-2 illustrates an example of a Newton white light interferometer and the resulting fringe pattern [19].
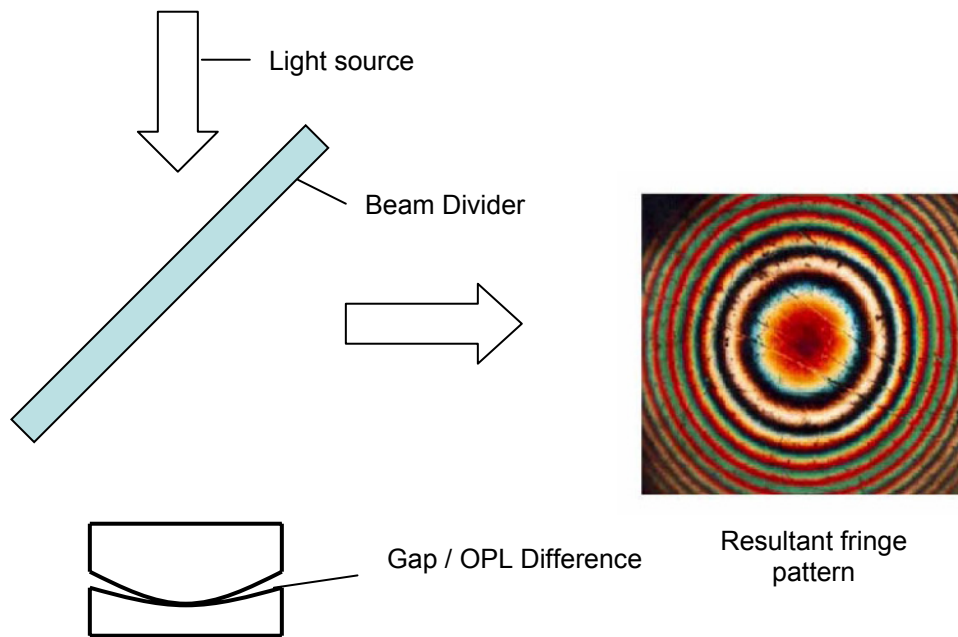
Figure 3-2: Newton white light interferometer and resulting fringe pattern [19]

The fringes seen in Figure 3-2 are a result of the constructive and destructive interferences that occur because of the varying gap size (and therefore OPL difference) between the two glass pieces. Because the gap size between the glass pieces is small, the two interfering beams remain sufficiently coherent to generate the fringe pattern shown in Figure 3-2. The fringes appear in several colors because the OPL difference at which constructive or destructive interference occurs varies according to wavelength. The gap size H may be described as a function of wavelength λ and fringe order N with the following equation

$$H = N \frac{\lambda}{2\cos\theta}$$
(3-1)

where θ is the angle of incidence which is zero for the configuration shown in Figure 3-2.

3.1.2 Need for verification of release agent delamination and adhesive bond interfacial delamination

The goal of the controlled area technique is to create a defined bond area from which interfacial delamination will consistently initiate from the bond's perimeter. However, when observing substrates after testing, it was not clear how initial failure took place. Because it was known that the release agent layer maintained some amount of adhesion, it was possible that once delamination was initiated between the release agent and substrate, the crack unstably propagated through the entire bond area. Such a scenario would be undesirable since it would only measure the force needed to initiate delamination at the release agent-substrate interface rather than at the adhesive-substrate interface. Another concern was the discovery that in the majority of cases, a portion of the adhesive remained on the substrate after delamination as shown in Figure 3-3.
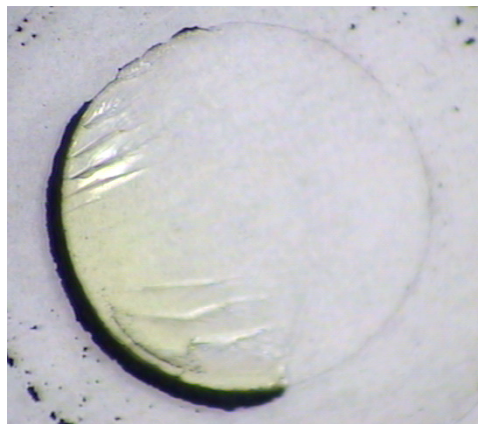
Figure 3-3: The substrate of a tested specimen showing some adhesive leftover

During delamination failures, it is not uncommon for delamination to initiate at one interface and propagate to another (or from inside the bulk material itself), while

leaving little evidence of what transpired. Therefore, a method was needed to observe the initiation and evolution of delamination along both the release agent layer and test adhesive substrate interfaces. The Newton style interferometer proved to be an ideal solution to this because of the ease in which it could be implemented and its ability to detect small gap sizes. Also, it should be noted that although the actual gap size could be determined with the observed fringe pattern, it was not of primary interest in this application. Only knowledge of the appearance of a fringe pattern which signifies the existence of some gap (and consequently delamination) was desired to be found out.

3.1.3 Application of white light interferometry to test geometry

Figure 3-4 depicts schematically how white light interferometry is applied to the specimen geometry and how the two incoming rays interfere in the presence of a gap at the release agent-substrate interface.
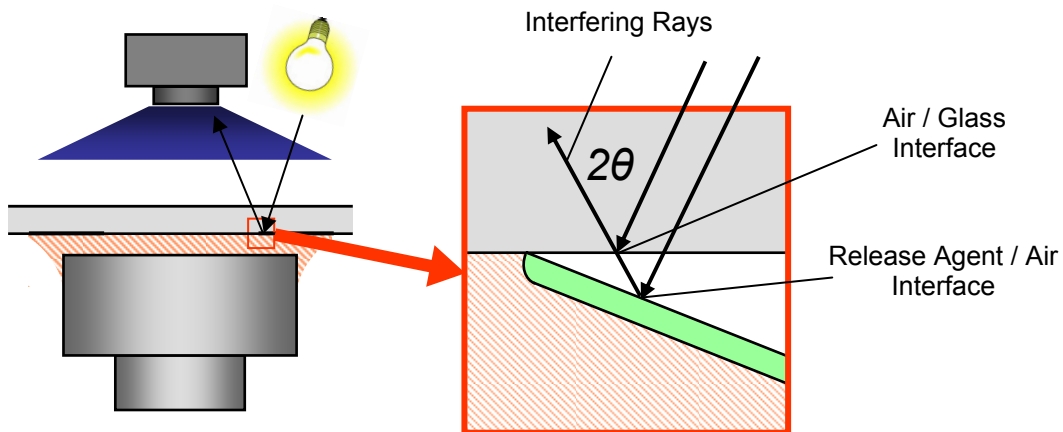
Figure 3-4: Schematic of the application of white light interferometry to the specimen geometry by placing the adhesion tester upside down

The presence of a gap at the release agent-substrate interface will cause interference because of the additional bimaterial interface that it creates. Without the existence of a gap, all incident light upon the substrate-adhesive or substrate-release agent interface will be reflected and traverse the same optical path length resulting in no interference. However, if an air gap is introduced as shown in Figure 3-4, a dielectric reflection will occur at the glass-air interface due to the differing indices of refraction between glass and air. A percentage of light will be transmitted through the glass-air interface while the rest will be reflected. As a result, two-beam interference can occur between the ray reflected from the glass-air interface and the trailing ray that is transmitted through the same interface.

The percentage of intensity of light reflected at the glass-air interface depends on the incident angle θ, ratio of the indices of refraction of the glass, and the polarization of the incident light [18]. If θ is too large (greater than approximately 40º for glass-air interfaces) total internal reflection will occur resulting in no optical interference or fringe patterns. If θ is too small, only a small amount of light will be reflected at the interface and a less than optimum fringe contrast will be observed. Therefore, in the experimental setup, the position of the P.A.T.T.I. adhesion tester had to be adjusted to an appropriate angle to obtain good fringe contrast. It was mounted on a tilt stage beneath the camera assembly. This can be seen in the experimental setup shown in Figure 3-5 .
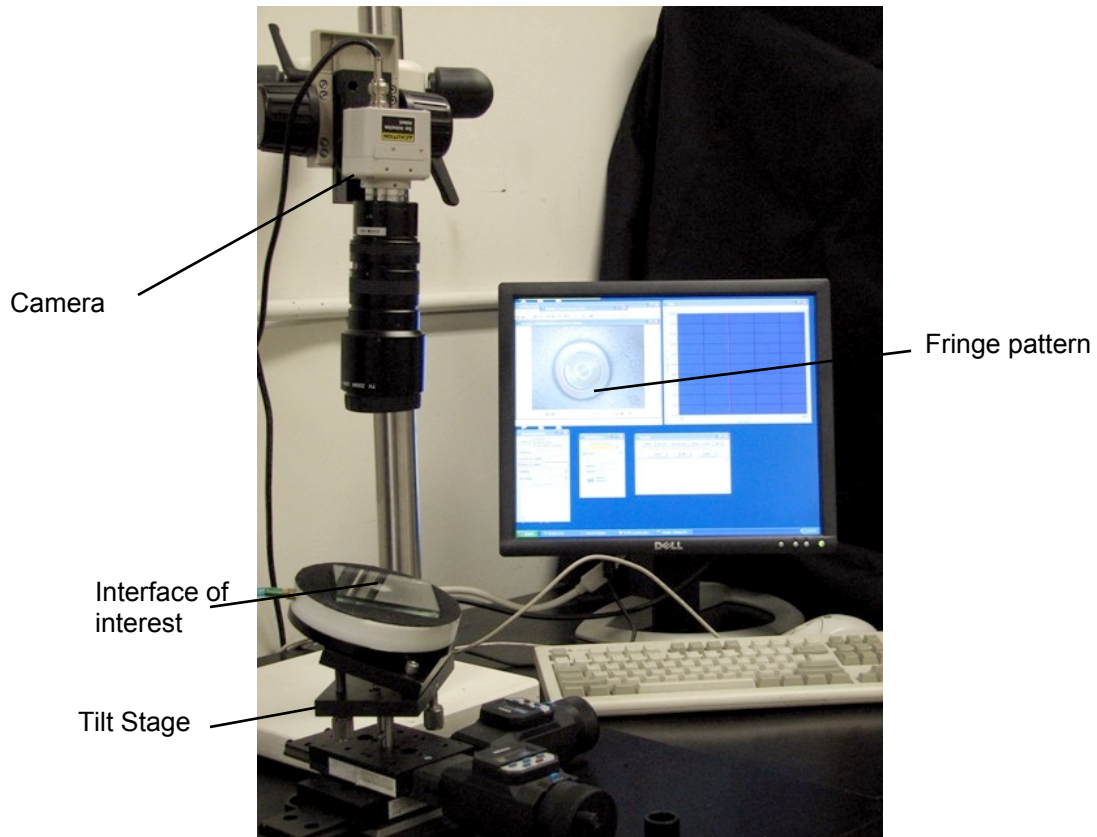
Figure 3-5: Experimental setup used for white light interferometry

3.1.4 Results and conclusions from white light interferometry

3.1.4.1 Verification of initial outer edge delamination

When the technique of white light interferometry was first used to observe the formation of crack growth along the interface, it was found that delamination from the outer release agent layer through the bulk adhesive was nearly instantaneous. This meant that the defined test area was not being used to characterize adhesion strength. In effort to resolve this, it was determined that the adhesion of the release agent layer was too high and should be reduced.

After successfully reducing the release agent strength, the interface was again observed during loading. The emergence of the fringe pattern that was seen is illustrated in Figure 3-6.
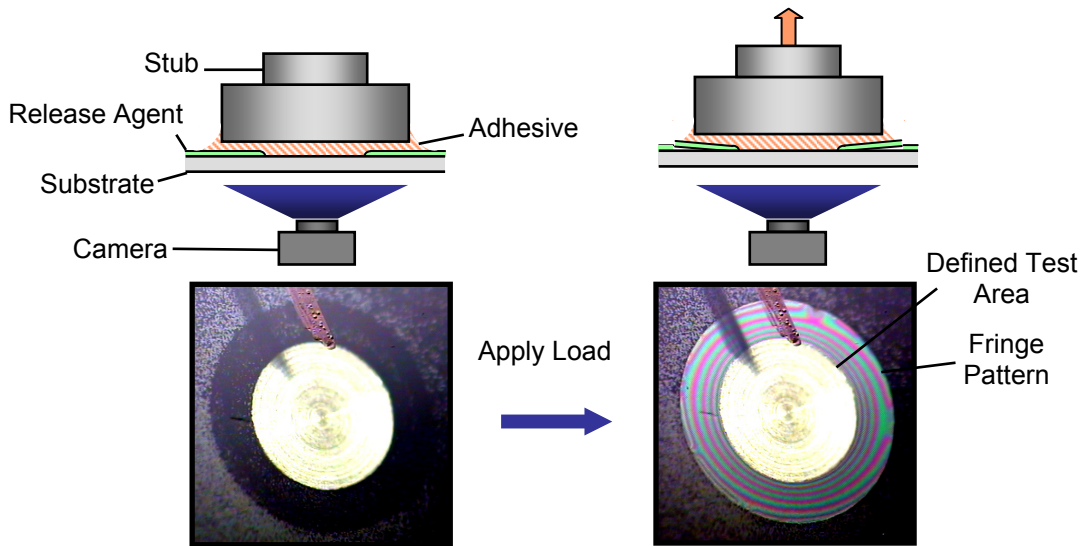
Figure 3-6: Before and after loading photographs of the adhesive bond area showing delamination in the region of the release agent

As explained in Section 3.1.3, the fringes verify the existence of a gap between the substrate-release agent interface indicating that delamination has occurred. This confirmed that the proposed controlled area technique was successful.

3.1.4.2 Real time observation of crack growth and failure in test specimens

As discussed in Section 3.1.2, knowledge of the site of failure initiation was previously unknown. Now by using white light interferometry during the testing procedure, the initial delamination process was able to be observed and is shown in Figure 3-7.
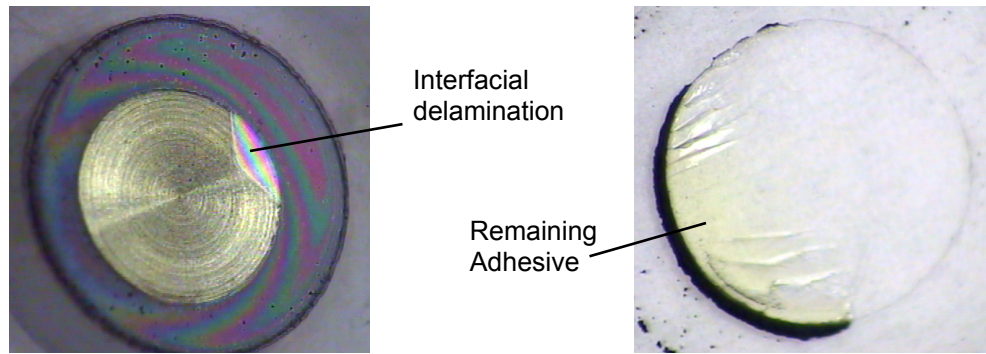
Figure 3-7: Location of initial interfacial delamination in the adhesive bond area in comparison to the location of remaining epoxy after testing

The migration of the fringe pattern into the adhesive bond area indicates that delamination is taking place interfacially between the substrate and adhesive. Also, it was seen upon post inspection of the substrate that the remaining adhesive was diametrically opposed to the site of initial failure. This indicates that delamination first occurred interfacially, and then propagated into the bulk of the adhesive. In the data that is reported in Chapter 3, all sites of failure initiation were observed to be opposite any remaining adhesive on the substrate. This was the desired outcome of the controlled area technique and is also what was predicted by the finite element model discussed in Section 3.2.2. But verification of the failure in real time was needed to assure confidence when testing nontransparent substrates, and has now been achieved.

3.2 Finite Element Analysis of Proposed Technique

A simple Finite Element Analysis (FEA) was performed to gain insight into several considerations during the design of the adhesion test including the anticipated location of failure, sensitivity of the maximum interface stress to mask size

uncertainty, sensitivity of the maximum interface stress to release agent thickness uncertainty, and the effect of substrate thickness on the maximum interface stress.

3.2.1 Overview of 2D axisymmetric model

The geometry of the model and the mesh used are shown in Figure 3-8 where (a) depicts the whole model geometry and (b) is an enlarged view of the interface.

.25"

Pressure Load

Pull Stub

Axis of Symmetry

Adhesive

Zero Displacement
Constraint

(a)
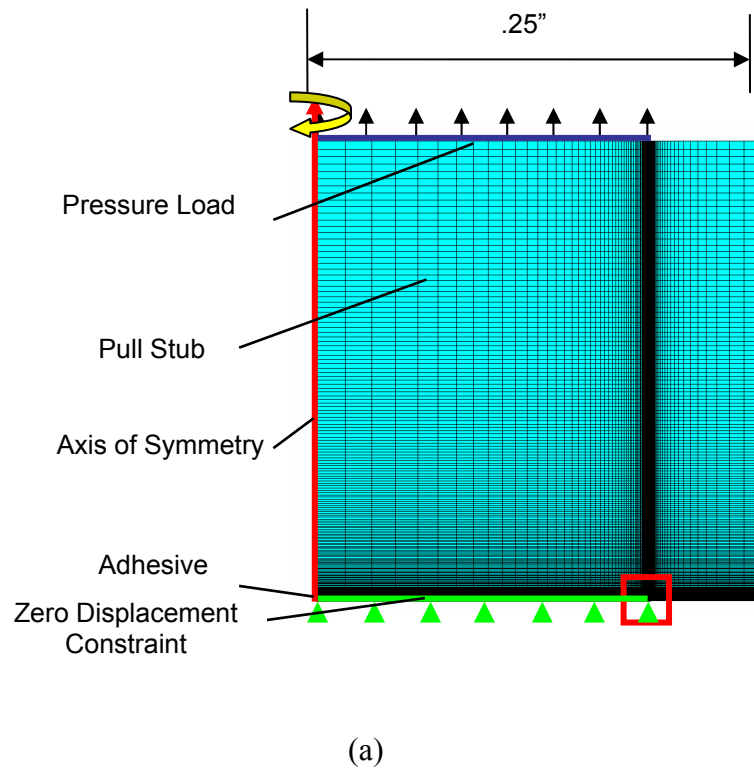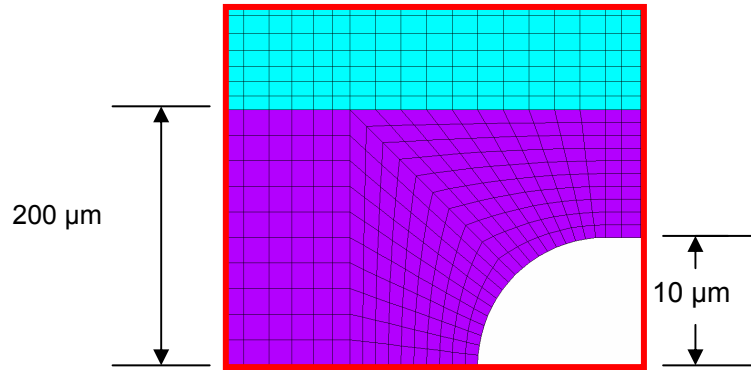
(b)

Figure 3-8: (a) Finite element mesh of entire model geometry showing loads and constraints and (b) enlarged view of mesh at the interface

The model takes advantage of the axisymmetric nature of the specimen geometry by utilizing a two degree of freedom axisymmetric PLANE82 element. All material properties are modeled as linear elastic isotropic. As may be seen in Figure 3-8, both the substrate and release agent materials were omitted to simplify the model. The substrate was assumed to be rigid and in its place a zero displacement constraint in the y direction was imposed along the bottom nodes of the adhesive layer. The release agent layer was neglected because of its low modulus and negligible effect on the interface stress when compared to those of the adhesive and substrate. Thicknesses of 200 μm for the adhesive and 10 μm for the release agent layer were used. A uniform tensile stress was applied to the top of the stub over 75% of its radial length to model the shaft axis of the stub. All of the FEA cases were performed in ANSYS 9.0.

3.2.2 Sensitivity of maximum interface stress to mask size

To facilitate the choice of the mask size diameter, a parametric analysis was performed to observe the rate of change of the maximum interface stress for several mask sizes. Since only the effect of a change in the adhesive bond area was to be observed, the load applied to the stub surface needed to be normalized for each corresponding bond area. This ensured that the same average interface stress along the substrate-adhesive bondline was used for each case. Ten mask sizes were analyzed in all. Contour plots showing the resulting stress distribution are shown in Figure 3-9 while the effects of multiple mask sizes on the maximum stress are shown in Figure 3-10.

(a)   (b)
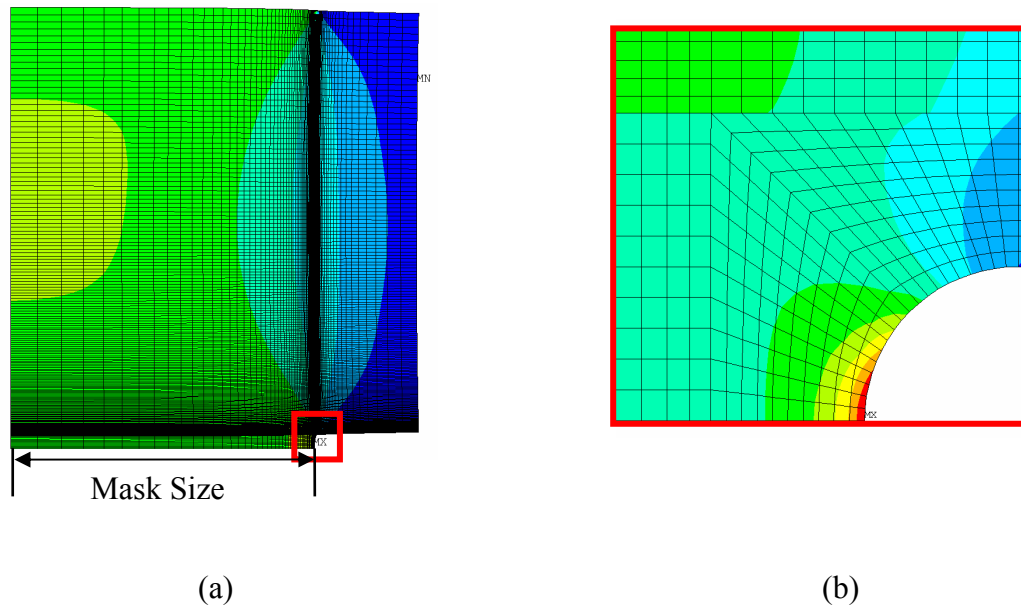
Figure 3-9: Contour plots showing the resulting Von Mises stress distribution in the (a) whole specimen geometry and (b) at the interface where the maximum stress occurs

Normalized σ_y at Interface vs. Mask Radius as Percentage of Total Stub Radius
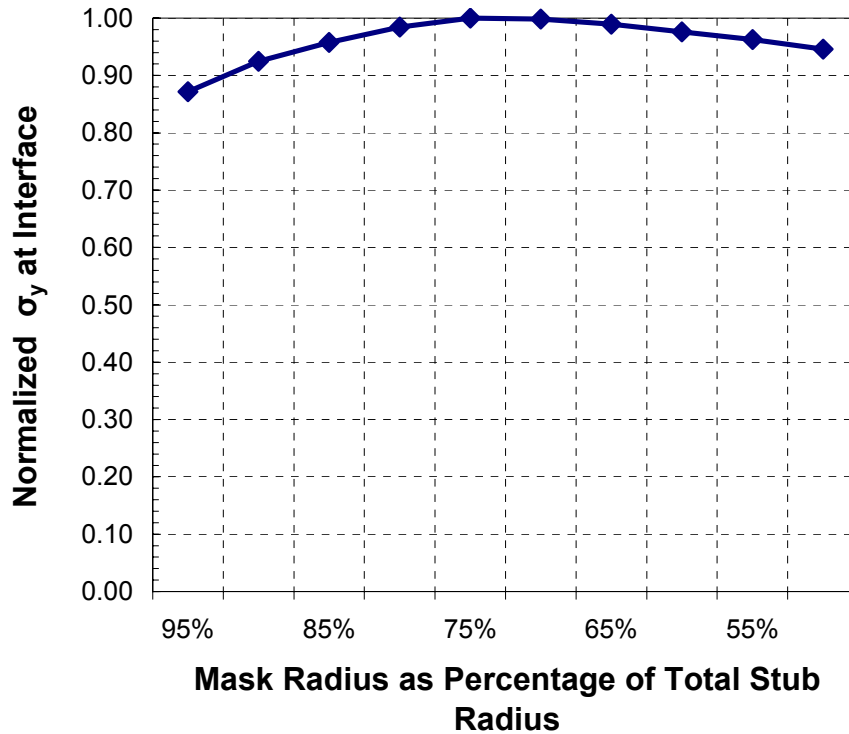
Figure 3-10: Plot of the maximum normalized stress at the interface vs. the percentage of the mask radius to the total stub radius

The results show that the maximum stress and initial delamination should occur at the substrate-adhesive interface as shown in Figure 3-9(b) which was later confirmed by using white light interferometry (Section 3.1.4.2). Figure 3-10 shows that by using a mask size of approximately 75% of the stub diameter, or 3/8", the change in maximum interface stress for some uncertainty in the mask size should be nearly zero. Additionally, 3/8" is a convenient dimension since the plastic washers which were found to be most suitable for the task of masking are only manufactured in discrete fractional increments.

3.2.3 Sensitivity of the maximum interface stress to release agent thickness

The sensitivity of the interface stress to the release agent thickness was also studied with a parametric variation of the release agent layer thicknesses. In these analyses, a mask size of 75% and an adhesive thickness of 200 μm were used. The results are shown in Figure 3-11.

Normalized y Component Stress vs. PVA Thickness (μm)
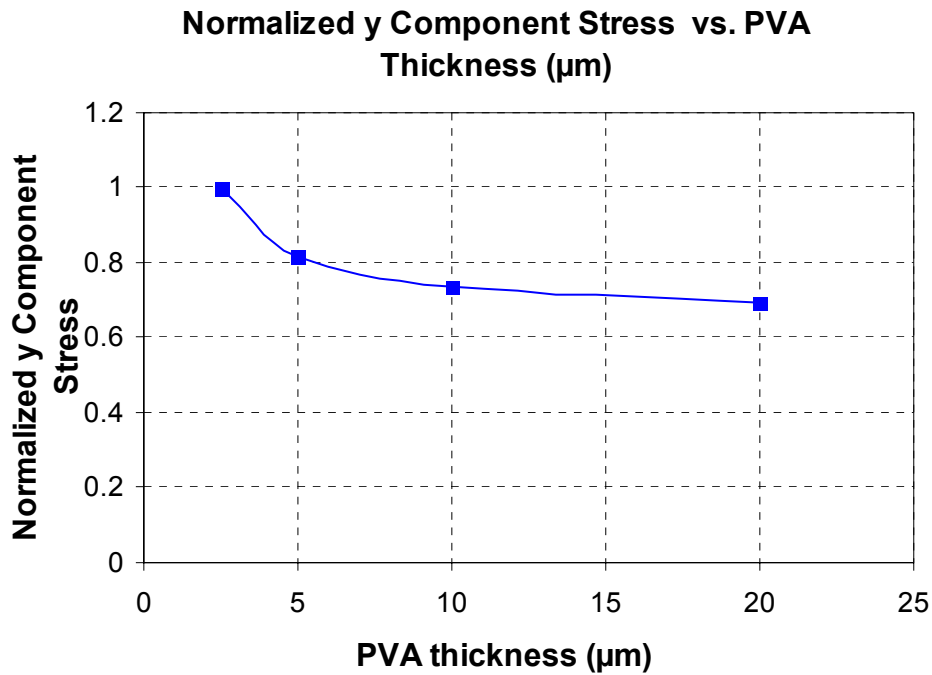
Figure 3-11: Normalized maximum y-component stress at the substrate-adhesive interface vs. PVA thickness (μm)

The results show that for increasing PVA layer thicknesses, changes in the maximum interface stress will decrease for a given absolute uncertainty in PVA thickness. Based on this relationship and the adhesion values obtained in Section 2.4.1, a release agent layer of approximately 12 μm was chosen for application.

CHAPTER 4: EXPERIMENTAL RESULTS

4.1   Adhesion strength data

4.1.1   Conventional adhesion test using PC-10C epoxy

To measure the effectiveness of the newly developed adhesion test, it was necessary

to characterize the performance of the conventional pull test for use as a control

sample set.   For testing, PC-10C liquid type epoxy (Photoelastic Division,

Measurement Groups Inc.) was used as the adhesive material. The preparation and

test procedures specified by the manufacturer of the P.A.T.T.I equipment were

followed to obtain the adhesion test results [20] and are a standardized adhesion test

procedure by ASTM [10]. None of the techniques developed to control the loading

rate or bond geometry described in Chapter 2 were used in the collection of this data.

The results for a sample of 40 trials are shown in Figure 4-1. The average adhesion

strength was found to be 848 PSI with a standard deviation of 431 PSI yielding a

percentage standard deviation of 50.1%. The data is plotted in Figure 4-1 normalized

to an average adhesion strength of one.

Normalized Adhesion Strength vs. Sample Number Using Conventional Adhesion Test and PC-10C Epoxy
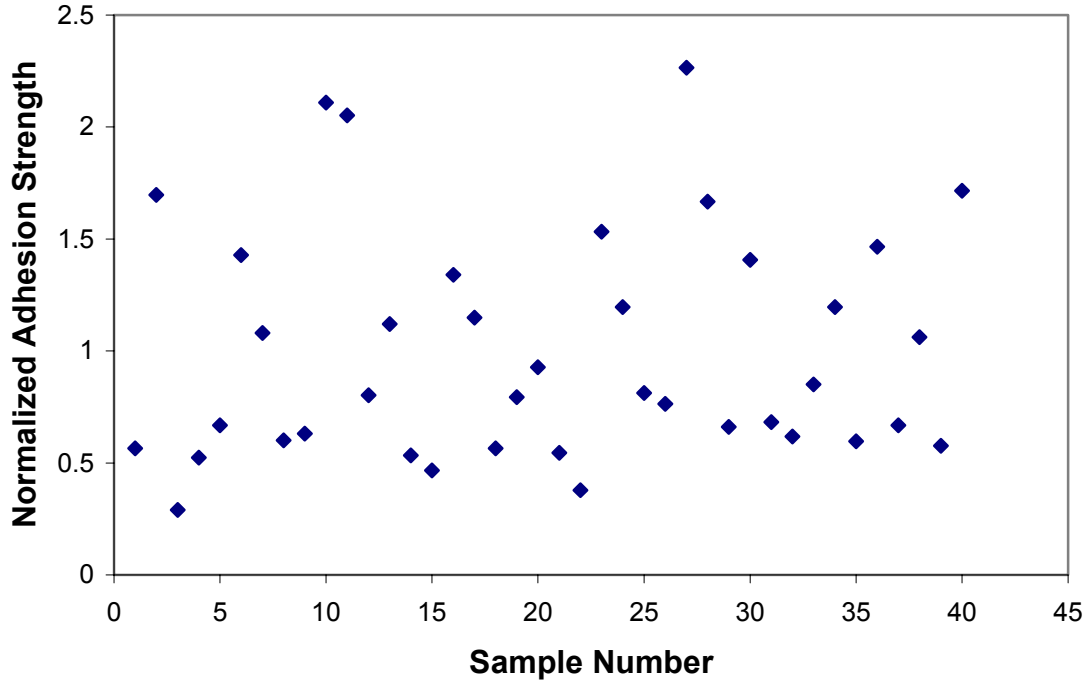
Figure 4-1: Adhesion test data obtained using the conventional adhesion test for PC-10C epoxy [15]

4.1.2 Advanced adhesion test using PC-10C epoxy

The PC-10C epoxy was also characterized with the advanced adhesion test by using all of the techniques described in Chapter 2. The results for a sample set of 16 trials are shown in Figure 4-2 with the data normalized to an average adhesion strength of one. The average adhesion strength was found to be 1640 PSI with a standard deviation of 151 PSI yielding a percentage standard deviation of 9.20%.

**Normalized Adhesion Strength vs. Sample Number Using
Advanced Adhesion Test for PC-10C Epoxy**
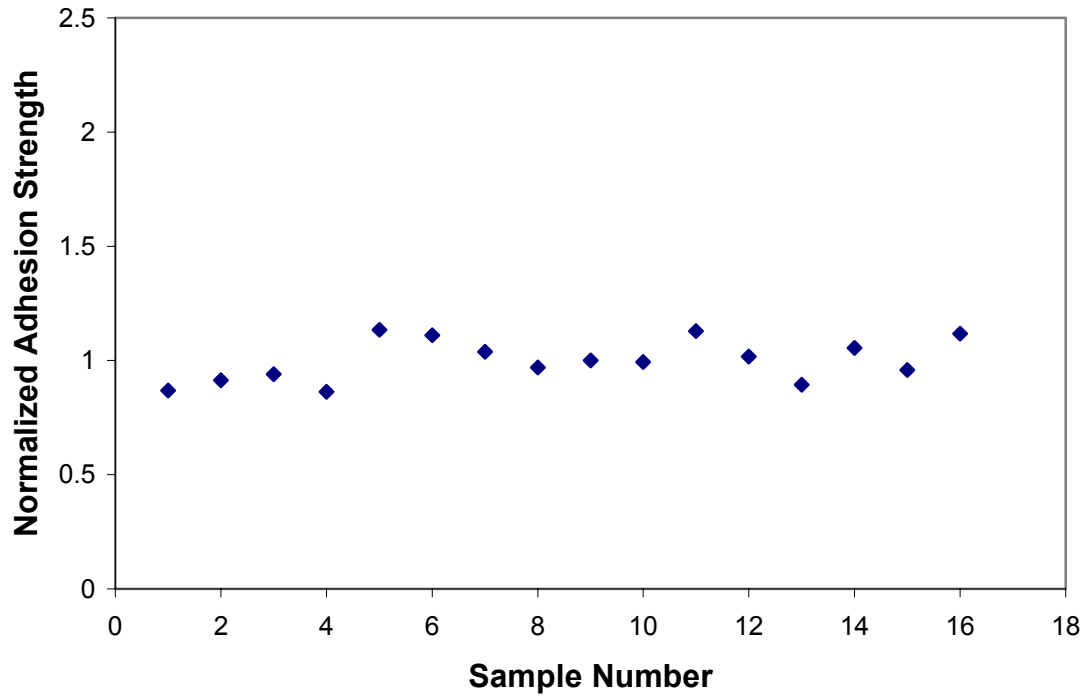
Figure 4-2: Adhesion test data obtained using the advanced adhesion test for PC-10C epoxy

4.1.3 Advanced adhesion test using Adwill LE4764 laminated adhesive

The advanced pull test was also used to measure the adhesion of a laminated type adhesive (Adwill LE4764). The preparation method used for the laminated adhesive is described in Section 2.3.4. The results are shown in Figure 4-3. The average adhesion strength was found to be 1070 PSI with a standard deviation of 66.7 PSI yielding a percentage standard deviation of 6.21%.

**Adhesion Strength (PSI) vs. Sample Number Using
Advanced Adhesion Test for Adwill LE4764 Adhesive**
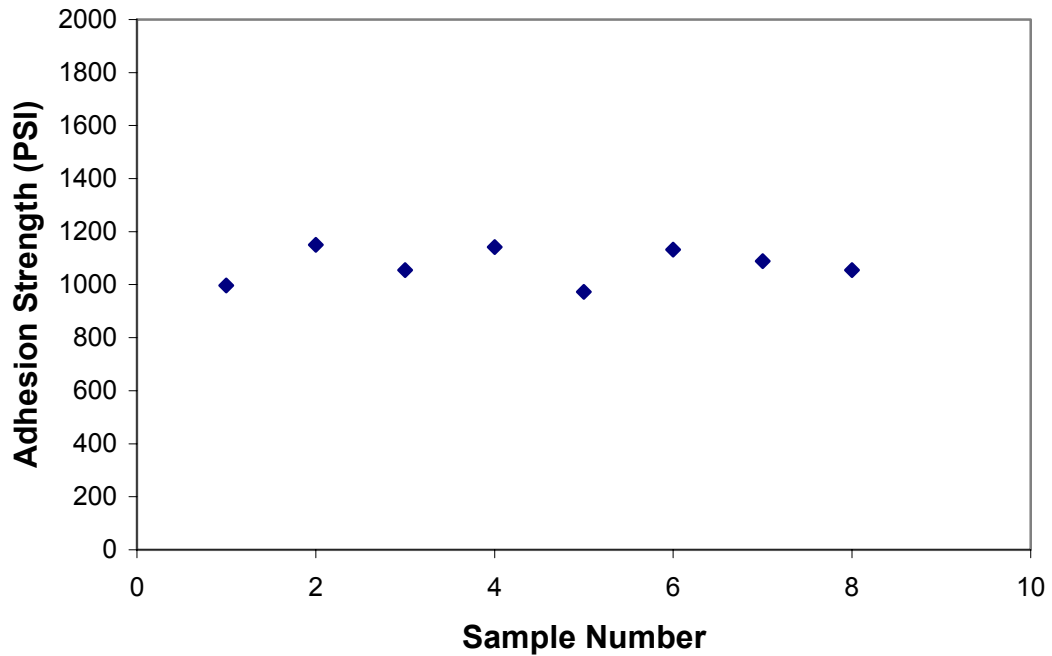
Figure 4-3: Adhesion test data obtained using the advanced adhesion for Adwill
LE4764 laminated adhesive

4.2   *Introduction to Analysis of Variance (ANOVA)*

To gain a better understanding into the significance of the reduction in deviation
between data reported in Sections 4.1.1 and 4.1.2, the one way ANOVA is performed.
A one-way ANOVA test is used to compare the means of two or more samples of
data to conclude if they are statistically the same or different. It is achieved by
determining if the amount of variation among the sample means is sufficiently large
compared to the amount of variation within the means. The null hypothesis H_0 for a
one-way ANOVA test states that the means of all the samples sets are equal. The null

hypothesis is rejected if the *F*-statistic calculated from the data is greater than the critical *F*-statistic F_α. The critical *F*-statistic is a function of the number of sample sets, the number of trials in each sample, and the significance level α. It can be determined by referencing an *F* distribution table [21]. The *F*-statistic that characterizes the sample data is defined as

$$F = \frac{MSTR}{MSE},$$

(4-1)

where *MSTR* is the treatment of mean square and *MSE* is the error mean square. The *MSTR* measures the variation among the sample means and is defined by

$$MSTR = \frac{SSTR}{k-1},$$

(4-2)

where *k* is the number of populations and *SSTR* is the treatment sum of squares defined as

$$SSTR = n_1\left(\overline{x}_1 - \overline{x}\right)^2 + n_2\left(\overline{x}_2 - \overline{x}\right)^2 + \mathrm{L} + n_k\left(\overline{x}_k - \overline{x}\right)^2.$$

(4-3)

In Equation 4-3, n_i and $\overline{x}_i$ are the number of trials and mean of the ith population, respectively, for $i=1, 2, \ldots, k$, and $\overline{x}$ is the average of all trials. To measure the variation in each sample set, the error mean square (*MSE*) is defined as

$$MSE = \frac{SSE}{n-k}, \qquad\qquad (4\text{-}4)$$

where n is the total number of trials and SSE is the error sum of squares defined as

$$SSE = (n_1 - 1)s_1^2 + (n_2 - 1)s_2^2 + L \ (n_k - 1)s_k^2. \qquad\qquad (4\text{-}5)$$

In Equation 4-5, s_i^2 is the variance in the ith population for i=1, 2, . . ., k. To summarize and keep account of these parameters, it is useful to construct a one-way ANOVA table like Table 4-1.

Source	Degree of Freedom (dof)	Sum of Squares (SS)	Mean Square (MS) = SS/dof	F-statistic
Treatment	k - 1	SSTR	$MSTR = \dfrac{SSTR}{k-1}$	$F = \dfrac{MSTR}{MSE}$
Error	n - k	SSE	$MSE = \dfrac{SSE}{n-k}$	

Table 4-1: One-way ANOVA table

For the following analyses, two hypothetical sample sets will be compared as if they were obtained from either the conventional adhesion test method or the advanced method. The two sample sets will be assumed to have the same standard deviation as their corresponding method reported in either Section 4.1.2 or 4.1.2 . For the conventional adhesion test, this is 50.1% and 9.2% for the advanced adhesion test. Since all analyses will only be between two samples sets, we may fix $k=2$. Also, to facilitate the analyses, it is convenient to express the mean of the second sample set

μ_2, as a ratio to the mean of the first sample set μ_1, such that $\mu_2 = \beta \mu_1$. In this same way, we may express $s_2 = \beta s_1$. Additionally, let the decimal equivalent of the percent standard deviation of the pair of sample sets be denoted as D. And since the purpose of the following analyses is to elicit comparative conclusions between two samples sets regardless of their absolute numerical mean values, μ_1 may be assigned to unity. By doing this, we may now express the key parameters in Table 4-1 that are used to determine the F-statistic in terms of β, D, and n. These relationships are shown in Table 4-2.

Source	dof	MS	F-statistic
Treatment	1	$MSTR = \dfrac{1}{2}n\left(\left(\dfrac{1}{2}-\dfrac{1}{2}\beta\right)^2+\left(\dfrac{1}{2}\beta-\dfrac{1}{2}\right)^2\right)$	$F = \dfrac{n(n-2)}{2}\dfrac{MSTR}{MSE}$
Error	$n-2$	$MSE = \left(\dfrac{1}{2}n-1\right)\left(1+\beta^2\right)D^2$	

Table 4-2: One-way ANOVA table as a function of β, n, and D.

4.2.1 ANOVA comparison of the conventional and advanced adhesion tests for the minimum discernable difference between two sample means

To determine the minimum discernable difference between two sample means μ_1 and μ_2 with percent deviation 50.1% that the conventional adhesion test reported in Section 4.1.2, the critical F-statistic F_α is first calculated. For a two sample set each with 40 trials, F_α is determined to be approximately 3.92 at the .05 significance level. And since n and D are known, the F-statistic as expressed in Table 4-2 can be solved

explicitly yielding a β of 1.26. This means that the difference between two sample means with standard deviation 50% and containing 40 trials each, must be greater than 26% to statistically differentiate them at the .05 significance level. Now the same treatment will be applied to the data obtained from the advanced adhesion test.

For two samples sets of 16 trials each obtained using the advanced adhesion test, a F_α of 4.16 at the .05 significance level is obtained. Letting D=.092 and solving for β in the manner described above, it is determined that β of approximately 1.07 is required to statistically differentiate the two means. Thus, the advanced adhesion test is able to 'resolve' the difference between two mean values to a difference of only 7% in their means compared to 26% with the conventional adhesion test, and it is able to do so with 24 fewer trials in each sample set.

To compare the performance of each technique using the same sample number of trials per sample set, let there be 10 trials per sample. Using the same analysis as above, we now find β for the conventional test to be 70% while β for the advanced test to be less than 10%. This demonstrates the substantial improvement in the ability of the advanced adhesion test to differentiate smaller differences in adhesion strength values.

4.2.2 A comparison between the conventional and advanced adhesion test for the minimum number of samples needed to discern between two sample means

Similar to the way β was solved for each test technique in Section 4.2.1, n can be determined for any given β. This will tell us the number of samples that are expected to be necessary to statistically discern between two adhesion strengths of ratio β. To do this, we determine the F–statistic and F_α in terms of D and β and then iterate n until the two values converge. The results of these calculations for four β's are shown in Table 4-3.

	Number of total trials needed n	
β	Conventional Test	Advanced Test
1.05	∞	58
1.10	∞	18
1.20	120	8
1.40	38	6

Table 4-3: Number of total trials n needed to differentiate between two sample means of ratio β at a significance of .05 using one-way ANOVA

The results shown in Table 4-3 demonstrate the value of the increased precision obtained with the advanced test. For example, to confidently differentiate sample means that differ by 5%, the conventional adhesion test would require an astronomical number of trials while the advanced test is able to achieve this with 58 trials. And to determine a more modest difference in sample means such as 20%, Table 4-3 shows that this would require a still very large sample set of 120 trials for the conventional adhesion test. Using the advanced test, this difference can be determined using a mere 8 trials. Thus it is easily seen how not only can the

advanced test measure smaller differences in sample means, but also how it greatly reduces the number of test trials that need to be performed to observe these differences. As a result, the time saved by using the advanced test could be used to either characterize more adhesives or to investigate the effects of outside variables on a particular adhesive-substrate system.

CHAPTER 5: FUTURE WORK

As a measurement technique, the advanced adhesion test was developed for the purpose of more precisely characterizing the adhesion between polymer interfaces. Therefore, the majority of work remains in the practice of the test towards the better characterization of adhesion of many materials interfaces. Due to the presence of a large amount of scatter previously associated with typical adhesion test data, the scope of analyses that could be carried out was limited. For example, performing a multivariable parametric analysis on adhesion strength to this point has largely been inaccessible due to the number of trials that would be needed to draw any statistically meaningful conclusions. But as demonstrated in Chapter 3, using the developed adhesion test with increased precision will allow one to make comparisons between adhesion strengths with greater confidence and accuracy, while simultaneously reducing the number of test trials that are needed to achieve this. As a result, several avenues of research in adhesion strength are now more feasible. From a packaging reliability stand point, topics of particular interest include effects from moisture, temperature, and fatigue on adhesion strength.

In addition to the future applications of the technique, there is work that may be done to further the development of the technique itself. For instance, parametric studies may be carried out to optimize parameters of the test procedure in attempt to reduce scatter even more, such as the stub size, adhesive bond thickness, release agent layer thickness, loading rate, or the ratio of bond area to stub area. Also, it has been

proposed that an investigation into the relationship between the adhesion strength and bond geometry be performed in an effort to develop an intrinsic material property utilizing fracture mechanics theory. The use of white light interferometry synchronized with pressure data from the PID controller would be prove to be useful in this regard for its ability to measure Mode I crack displacement as a function of the applied load.

And lastly, as with any measurement technique, it is important to understand how the adhesion strengths obtained correlate to the adhesive performances of bimaterial interfaces in real world systems. To do this, a degree of testing must be done to elucidate these relationships, which should now be accelerated by a measurement technique that can provide greater precision in less time.

CHAPTER 6: CONCLUSIONS

In Chapter 1, an investigation into the primary forms of adhesion testing was performed, comparing their advantages and disadvantages for the purpose of selecting an appropriate technique for the development of a test with increased precision. The pull test was selected, and the control of load alignment, loading rate, and the bond geometry were identified as primary factors contributing to the variance in its test results. Chapter 2 discussed the techniques that the advanced adhesion test uses to control the identified sources of variance emphasized in Chapter 1. A complete account of the experimental setup used to accomplish this was given, as well as a detailed experimental procedure for reproducing the results that were reported in Chapter 4.

In Chapter 3, a description was given on how white light interferometry was used to deduce that a better release agent was needed to successfully create a controlled bond area. After this was accomplished, the interferomic technique was then able to confirm the complete delamination of the outer release layer prior to the initiation of debonding in the adhesive area. White light interferometry was also used to determine that all observed adhesive delaminations occurred interfacially, as was predicted by the finite element analysis.

The newly developed adhesion test was applied to the measurement of a commercially available epoxy and compared to results obtained using a conventional

test that is standardized by ASTM. The results showed a reduction in percent deviation of 50% when using the conventional technique to less than 10% for the advanced adhesion test. A laminated type adhesive was also tested and yielded a percent deviation of only 6.2%. A one-way ANOVA analysis was conducted to illustrate the value of a measurement technique with increased precision. It highlighted both its ability to discern smaller differences between two sample means for a given number of trials, and also its ability to reduce the number of samples needed to discern a given difference in two sample means while maintaining equivalent statistical confidence.

The developed advanced adhesion test was demonstrated to successfully reduce the scatter associated with the pull test. This will allow more confident conclusions to be made between measured adhesion strengths, but perhaps more importantly save time by reducing the number of trials needed to do so. Because of this, it is now more practical to use adhesion testing in parametric analyses to understand important reliability problems like the effects of moisture, fatigue, and temperature on adhesion. The new information obtained from these analyses may yield improved adhesive properties for packaging materials that could be used to improve predictive reliability modeling.

Appendix A: ANSYS input command code used for generation and loading of finite element model described in Section 3.2.1

```
!new geometry with filleted pva edge and removal of glass substrate,
constrain adhesive base instead
!/clear
!/filname,fillet,db

!*********************************************
! parameter setup
!*********************************************
!Assumptions and parameters - Axisymmetric, PLANE82 element/8 node
element w/2 degrees of freedom, linear elastic

d1=0.000001

!GEOMETRIC PARAMETERS

!Adhesive_thickness=0.010
!PVA_thickness=0.000394                      ! about 10 micron
!Stub_radius=1.0                !(.25")
!Interior_radius=0.8*Stub_radius    !(.125"), should be a multiple
of
!Stub_axis=.375/2
Plate_thickness=0.123
Stub_height=0.25
Burst_press=5*(Interior_radius*Interior_radius)/(Stub_axis*Stub_axis
) !Input PSI, coverts to equivalent on shaft area, normalize to area
Plate_radius=1.25
stress_adhesive=Burst_press*(Stub_axis*Stub_axis)/(Interior_radius*I
nterior_radius) !(equals coefficient in burst_pressure)

! positions
x1=Interior_radius - PVA_thickness
x2=Interior_radius
x3=Interior_radius + PVA_thickness
x4=Stub_radius
x5=Plate_radius

y1=Plate_thickness
y2=y1+PVA_thickness
y3=y2+PVA_thickness
y4=y3+Adhesive_thickness
y5=y4+Stub_height

!*********************************************
! element and material setup
!*********************************************

/prep7
```

```
! element setup
ET,1,PLANE82,,,1,,0              ! 183 is better than 82 for nonlinear
analysis
!
! material properties
! 1: Al, 2: Adhesive, 3: PVA, 4: glass substrate
!Aluminum
MP,EX,1,10.15e6          !70e9 Pa
MP,NUXY,0.33

!Adhesive
MP,EX,2,20001            !137.9e6 pa, From CW's code
MP,NUXY,2,0.3

!PVA
MP,EX,3, 50763           !3.5E8,
http://scitation.aip.org/journals/doc/APPLA-
/vol_86/iss_11/113104_1.html#F2
MP,NUXY,3,0.48

!Glass Substrate
MP,EX,4,10399205*10000   !Fused Quartz/Silica 71.7 Gpa, v=.16, make
rigid for parametric study
MP,NUXY,4,0.16

!*******************************************
! geometric modeling
!*******************************************

!first build not extrudable geometry/fillet

k, 1, x1, y1
k, 2, x3, y2,
k, 3, x3, y3
k, 4, x1, y3
k, 5, x3, y1             !arc center
k, 6, x3, y1, 1          !defines axis of rotation

lrotat,2,,,,,,5,6,90,2
l, 1, 8
l, 1, 4
l, 4, 3
l, 3, 2
l, 4, 7

al, 3, 4, 7, 2
al, 5, 6, 1, 7

!now create lines to extrude for the rest of the geometry

!lines along stub axis
k,100,0,0
k,200,0,y1
k,300,0,y3
k,400,0,y4
k,500,0,y5
l,100,200   !line8
```

```
l,200,300   !line9
l,300,400   !line10
l,400,500   !line11

!lines along x axis
k,600,x1,0
k,700,x2,0
k,800,x4,0
k,900,x5,0
l,100,600   !line12
l,600,700   !line13
l,700,800   !line14
l,800,900   !line15

!lines along top of stub
k,1000,x1,y5
k,1100,x3,y5
k,1200,x4,y5
k,1300,x5,y5
l,500,1000  !line16
l,1000,1100 !line17
l,1100,1200 !line18

!extrude areas
adrag,8,,,,,,12,13,14,15
adrag,9,,,,,,12
adrag,10,11,,,,,16,17,18
BLC4,x3,y2,x4-x3,PVA_thickness
aglue,all              !glue all areas for meshing preparation

!AREA ATTRIBUTION
asel,,loc,y,,y1
aatt,4
asel,,loc,y,y1,y3
asel,u,mat,,3
aatt,2
asel,,loc,y,y3,y4
aatt,1

!*******************************************
! Meshing
!*******************************************

!set line divisions
!LESIZE, NL1, SIZE, ANGSIZ, NDIV, SPACE, KFORC, LAYER1, LAYER2,
KYNDIV

!by varying line divisions by same amount, this keeps the aspect
ratio of the small element at the interface constant
pi=3.1415926535897
!ndivs=5    !number of divisions along fillet
element_length_x = PVA_thickness/ndivs
element_length_y = pi*PVA_thickness/(4*ndivs)

!set mesh for fillet area, need to be careful about element size
when measuring stress
lsel,,line,,1
```

```
lsel,a,line,,2
lesize,all,,,ndivs

lsel,,line,,3
lsel,a,line,,6
lesize,all,,,ndivs                  !not needed when assigning sizes
to line 7

!lsel,,line,,7                      !not needed because of divisions
assigned to opposite side
!lesize,all,3*PVA_thickness/20,,,1/2

!Rest of geometry
lsel,,loc,x,d1,x1-d1               !inner radius horizontal lines
lsel,r,loc,y,y1-d1,y3+d1
lesize,all,301*element_length_x/4,,,300

lsel,,loc,x,d1,x1-d1               !line spacing is reversed for
some reason
lsel,u,loc,y,y1-d1,y3+d1
lesize,all,301*element_length_x/4,,,1/300

lsel,,loc,x,x3+d1,x4-d1           !upper right horizontal lines
lsel,r,loc,y,y2-d1,y5+d1
lesize,all,201*element_length_x/4,,,200

lsel,,loc,x,x2+d1,x4-d1           !lower middle horizontal lines
lsel,r,loc,y,-d1,y1+d1
lesize,all,201*element_length_x/4,,,200

lsel,,loc,x,x4+d1,x5-d1           !horizontal lines along plate
lesize,all,900*element_length_x,,,4

lsel,,loc,y,d1,y1-d1              !vertical lines in substrate
lsel,r,loc,x,x1-d1,x2+d1
lesize,all, 201*element_length_y/4,,,200

lsel,,loc,y,d1,y1-d1              !line spacing is reversed for
some reason
lsel,u,loc,x,x1-d1,x2+d1
lesize,all, 201*element_length_y/4,,,1/200

lsel,,loc,y,y3+d1,y4-d1          !adhesive thickness vertical
lines
lesize,all, 11*element_length_y/2,,,10

lsel,,loc,y,y4+d1,y5-d1          !stub vertical lines
lesize,all, 10*11*element_length_y/2,,,10

mshkey,1                        ! map meshing
asel,all
amesh,all



!~20k elements
```

```
!*********************************************
! loading and solving
!*********************************************

/sol

nsel,,loc,x,-d1,d1        !create component to assign symmetry boundry
condition on y axis
cm,x_fix,node
d,x_fix,ux,0

nsel,,loc,y,y5-d1,y5+d1 !create component to apply pressure to stub,
thread radius is .375/2"
nsel,r,loc,x,-d1,Stub_axis-d1
cm,n_press,node
sf,n_press,press,-Burst_press
!CMSEL,S,N_PRESS                !select nodes to couple
!CP,1,UY,all                        !couple in y direction, 1 is an
arbitrary number assigned to command

alls

!Removing plate and contraining adhesive instead in this case
!nsel,,loc,y,-d1,d1       !create component to constrain nodes on
bottom of plate
!cm,plate_fix,node
!d,plate_fix,uy,0

nsel,,loc,x,-d1,x2+d1
nsel,r,loc,y,y1-d1,y1+d1
cm,adhesive_fix,node
d,adhesive_fix,uy,0

allsel
esel,u,mat,,4      !unselect substrate, not necessary

solv

!*********************************************
! post-processing
!*********************************************

/post1
set,last

nsel,,loc,x,x2-d1,x2+d1                !get node number at interface
nsel,r,loc,y,y1-d1,y1+d1
*get,n_interface,node,,num,max

esel,,mat,,2                            ! MUST select adhesive only for
prevent averaging at interface
plns,s,1

*dim,s_result,array,3,1             ! array to store stress values
*get,s_result(1,1),node,n_interface,s,1
*get,s_result(2,1),node,n_interface,s,y
*get,s_result(3,1),node,n_interface,s,eqv
```

78

```
*get,title1,active,,jobnam
/output,stress_result,out,,append          ! works only at batch mode
*stat,title1
*stat,s_result
*stat,stress_adhesive
*stat,element_length_x
*stat,element_length_y
*stat,ndivs
/output
```

Appendix B: ANSYS Parametric Design Language (APDL) code used to run parametric analysis described in Section 3.2.2

```
fini
/clear
/filname,model1,db
Adhesive_thickness=200/25400
PVA_thickness=0.000394
Stub_radius=0.25
Interior_radius=.95*Stub_radius
Stub_axis=.375/2
ndivs=10
/input,newgeom_fillet_noglass_fullstub_axisloading,txt

fini
/clear
/filname,model1,db
Adhesive_thickness=200/25400
PVA_thickness=0.000394
Stub_radius=0.25
Interior_radius=.90*Stub_radius
Stub_axis=.375/2
ndivs=10
/input,newgeom_fillet_noglass_fullstub_axisloading,txt

fini
/clear
/filname,model1,db
Adhesive_thickness=200/25400
PVA_thickness=0.000394
Stub_radius=0.25
Interior_radius=.85*Stub_radius
Stub_axis=.375/2
ndivs=10
/input,newgeom_fillet_noglass_fullstub_axisloading,txt

fini
/clear
/filname,model1,db
Adhesive_thickness=200/25400
PVA_thickness=0.000394
Stub_radius=0.25
Interior_radius=.80*Stub_radius
Stub_axis=.375/2
ndivs=10
/input,newgeom_fillet_noglass_fullstub_axisloading,txt

fini
/clear
/filname,model1,db
Adhesive_thickness=200/25400
PVA_thickness=0.000394
Stub_radius=0.25
Interior_radius=.75*Stub_radius
```

```
Stub_axis=.375/2
ndivs=10
/input,newgeom_fillet_noglass_fullstub_axisloading,txt

        fini
/clear
/filname,model1,db
Adhesive_thickness=200/25400
PVA_thickness=0.000394
Stub_radius=0.25
Interior_radius=.70*Stub_radius
Stub_axis=.375/2
ndivs=10
/input,newgeom_fillet_noglass_fullstub_axisloading,txt

        fini
/clear
/filname,model1,db
Adhesive_thickness=200/25400
PVA_thickness=0.000394
Stub_radius=0.25
Interior_radius=.65*Stub_radius
Stub_axis=.375/2
ndivs=10
/input,newgeom_fillet_noglass_fullstub_axisloading,txt

        fini
/clear
/filname,model1,db
Adhesive_thickness=200/25400
PVA_thickness=0.000394
Stub_radius=0.25
Interior_radius=.60*Stub_radius
Stub_axis=.375/2
ndivs=10
/input,newgeom_fillet_noglass_fullstub_axisloading,txt

        fini
/clear
/filname,model1,db
Adhesive_thickness=200/25400
PVA_thickness=0.000394
Stub_radius=0.25
Interior_radius=.55*Stub_radius
Stub_axis=.375/2
ndivs=10
/input,newgeom_fillet_noglass_fullstub_axisloading,txt

        fini
/clear
/filname,model1,db
Adhesive_thickness=200/25400
PVA_thickness=0.000394
Stub_radius=0.25
Interior_radius=.50*Stub_radius
Stub_axis=.375/2
ndivs=10
```

Appendix C: ANSYS Parametric Design Language (APDL) code used to run parametric analysis described in Section 3.2.3

```
!75%

fini
/clear
/filname,model1,db
Adhesive_thickness=50/25400
PVA_thickness=0.000394
Stub_radius=0.25
Interior_radius=.75*Stub_radius
Stub_axis=.375/2
ndivs=10
/input,newgeom_fillet_noglass_fullstub_axisloading,txt

fini
/clear
/filname,model1,db
Adhesive_thickness=100/25400
PVA_thickness=0.000394
Stub_radius=0.25
Interior_radius=.75*Stub_radius
Stub_axis=.375/2
ndivs=10
/input,newgeom_fillet_noglass_fullstub_axisloading,txt


fini
/clear
/filname,model1,db
Adhesive_thickness=150/25400
PVA_thickness=0.000394
Stub_radius=0.25
Interior_radius=.75*Stub_radius
Stub_axis=.375/2
ndivs=10
/input,newgeom_fillet_noglass_fullstub_axisloading,txt


fini
/clear
/filname,model1,db
Adhesive_thickness=200/25400
PVA_thickness=0.000394
Stub_radius=0.25
Interior_radius=.75*Stub_radius
Stub_axis=.375/2
ndivs=10
/input,newgeom_fillet_noglass_fullstub_axisloading,txt


fini
/clear
```

```
/filname,model1,db
Adhesive_thickness=250/25400
PVA_thickness=0.000394
Stub_radius=0.25
Interior_radius=.75*Stub_radius
Stub_axis=.375/2
ndivs=10
/input,newgeom_fillet_noglass_fullstub_axisloading,txt
```

Bibliography

1. Ulrich, R. K., Brown, W. D., *Advanced Electronic Packaging*, IEEE, Inc., (Piscataway, NJ 2006), pp. 46.

2. Stellrecht, E., and Han, B., "Characterization of Hygroscopic Swelling Behavior of Mold Compounds and Plastic Packages," *IEEE Transactions on Components and Packaging Technology*, Vol. 27, No. 3 (September 2004).

3. Murray, S., Hillman, C., and Pecht, M., "Environmental Aging and Deadheasion of Siloxane-Polymide-Epoxy Adhesive," *IEEE Transactions on Components and Packaging Technology*, Vol 26, No 3 (September 2003).

4. Ferguson, T., and Qu, J., "An Engineering Model for Moisture Degradation of Polymer/Metal Interfacial Fracture Toughness," *Ph.D. Dissertation,* Georgia Institute of Technology (2004).

5. Frantzis, P., "Environmental Attack on Adhesive Joints," *JSME International Journal*, Series A, Vol 41, No. 2 (1998).

6. ASTM Standard Terminology of Adhesives, D 907-04.

7. Comyn, J., *Adhesion Science*, The Royal Society of Chemistry, (Cambridge, 1997), pp 4-10, 125.

8. Mittal, K. L. ed., "Adhesion Measurement of Films and Coatings: A Commentary," *Adhesion Measurement of Films and Coatings,* © VSP (1995), pp. 1-13.

9. ASTM Standard Test Method for Tensile Strength of Adhesives by Means of Bar and Rod Specimens, D 2095 – 96.

10. ASTM Standard Test Method for Pull-Off Strength of Coatings Using Portable Adhesion Testers, D 4541 – 02.

11. Anderson, G. P., Brinton, D. H., Ninow, K. J., and DeVries, K. L., "A Fracture Mechanics Approach to Predicting Bond Strength."

12. Van Tooren, M. J. L., Gleich, D. M., and Beukers, A., "Experimental Verification of a Stress Singularity Model to Predict the Effect of Bondline Thickness on Joint Strength," *Journal of Adhesion Science Technology*, Vol 18, No. 4, pp. 395-412 (2004).

13. Suo, Z., "Singularities Interacting With Interfaces and Cracks," *International Journal of Solids and Structures,* Vol. 25, No. 10 (1989), pp. 1133-1142.

14. Gladkov, A., and Bar-Cohen, A., "Parametric Dependence of Fatigue of Electronic Adhesives," *IEEE Transactions on Components and Packaging Technology,* Vol. 22, No. 2 (June 1999).

15. Han, C. W., and Han, B., "Development of Advanced Adhesion Test," *CALCE Electronic Products and Systems Center Conference,* C01-09 (Spring 2001).

16. Fisher, "Apparatus for Testing the Bond Strength of Materials," *United States Patent 4,567,758,* February 4, 1986.

17. Cox, A., "Development of Advanced Warpage Measurement Systems: Shadow Moiré with Nonzero Talbot Distance and Far Infrared Twyman-Green Interferometry," *M.S. Thesis,* University of Maryland – College Park (2006).

18. Post, D., Han, B., and Ifju, P., *High Sensitivity Moiré: Experimental Analysis for Mechanics and Materials,* Springer-Verlag (New York, 1994).

19. Wyant, J. C., *"White Light Interferometry."*

20. SEMicro Division M.E. Taylor Engineering, Inc., *PATTI ® 110 - Coatings and Adhesive Tester: Operator's Manual*.

21. Wilson, C. ed., *Experimental Design, ANOVA, and Regression,* Harper and Row, (New York, NY, 1987).